BRNO UNIVERSITY OF TECHNOLOGY
VYSOKÉ UČENÍ TECHNICKÉ V BRNĚ

FACULTY OF MECHANICAL ENGINEERING
FAKULTA STROJNÍHO INŽENÝRSTVÍ

INSTITUTE OF PHYSICAL ENGINEERING
ÚSTAV FYZIKÁLNÍHO INŽENÝRSTVÍ

MULTIFUNCTIONAL SNOM PROBES OF NEW GENERATION FOR CORRELATIVE SEM/SPM MEASUREMENTS

MULTIFUNKČNÍ SNOM SONDY NOVÉ GENERACE PRO KORELATIVNÍ SEM/SPM MĚŘENÍ

BACHELOR'S THESIS
BAKALÁŘSKÁ PRÁCE

AUTHOR — **Lukáš Zezulka**
AUTOR PRÁCE

SUPERVISOR — **prof. RNDr. Jiří Spousta, Ph.D.**
VEDOUCÍ PRÁCE

BRNO 2021

BRNO UNIVERSITY OF TECHNOLOGY
FACULTY OF MECHANICAL ENGINEERING

Assignment Bachelor's Thesis

Institut:	Institute of Physical Engineering
Student:	**Lukáš Zezulka**
Degree programm:	Applied Sciences in Engineering
Branch:	Physical Engineering and Nanotechnology
Supervisor:	**prof. RNDr. Jiří Spousta, Ph.D.**
Academic year:	2020/21

As provided for by the Act No. 111/98 Coll. on higher education institutions and the BUT Study and Examination Regulations, the director of the Institute hereby assigns the following topic of Bachelor's Thesis:

Multifunctional SNOM probes of new generation for correlative SEM/SPM measurements

Brief Description:

The bachelor's thesis will deal with a complex problem of enhancing designs and manufacturing unique hollow probes for Scanning Probe Microscopes (SPM), which, unlike what exists, would bring to the probes a higher degree of their functionality. In addition to commonly available analytical techniques such as measuring the topography and optical properties of surfaces and nanostructures in the distances lower than wavelength of the incoming light, will be studied possibilities of (besides the light) working fluids to be supplied to the vicinity of the probe tip and applying various voltages. These probes should be designed for simultaneous (correlative) measurements using scanning electron microscopy (e.g. in VEGA electron microscope from Tescan Brno company and SPM LiteScope from NenoVision company).

Bachelor's Thesis goals:

Search in the literature for the use of hollow fibres to introduce light and working fluids into the vicinity of the probe tip.
Explore possibilities of enhancing the current multifunctional probe for SNOM measurements with the possibility of a transport of the working fluid to the vicinity of the probe tip.
Optimize characteristic properties of multifunctional hollow SNOM probes using simulations in COMSOL programme (e.g. supplying of light and gas through capillaries)
Prepare the tip with a focused ion beam technique (FIB).
Perform correlative measurements with a new probe in the electron microscope chamber.

Recommended bibliography:

HOSSEIN-BABAEI, Faramarz, Ali HOOSHYAR ZARE a Vahid GHAFARINIA. Transient molecular diffusion in microfluidic channels: Modeling and experimental verification of the results. Sensors and Actuators B. 2016, (233), 646-653. ISSN 0925-4005.

PARMAR, Vinod a Randhir BHATNAGAR. Analysis of gas flow dynamics in hollow core photonic crystal fibre based gas cell. Optik. 2014, (125), 3204-3028. ISSN 0030-4026.

LIN, Yiliang, Olivia GORDON a M. Rashed KHAN. Vacuum filling of complex microchannels with liquid metal. Lab On a Chip. 2017, (18), 3043-3050. ISSN 1473-0197.

Deadline for submission Bachelor's Thesis is given by the Schedule of the Academic year 2020/21

In Brno,

L. S.

prof. RNDr. Tomáš Šikola, CSc.
Director of the Institute

doc. Ing. Jaroslav Katolický, Ph.D.
FME dean

ABSTRACT

Thesis deals with the drafted multifunctional SNOM probe for correlative SEM/SPM measurements utilising hollow optical fibre with a solid core. In the research part are examined possible means of SNOM tip fabrication on a hollow fibre, the appliance of the hollow capillaries to bring working fluids to the sample, and available solutions for introducing a potential difference to the sample via capillaries filled with conductive material. Furthermore, a developed SNOM tip fabrication process is presented and the whole concept is proven to be functional with performed correlative measurements. Consequentially problems occurring during the fabrication and measurements are discussed.

KEYWORDS

SEM, SPM, SNOM, solid core photonic crystal fibre, gas flow

ABSTRAKT

Práce se věnuje návrhu multifunkční SNOM sondy pro korelativní SEM/SPM měření využívající dutého optického vlákna s plným jádrem. V rešerši jsou prozkoumány možné způsoby výroby SNOM hrotů na dutém optickém vlákně, využití dutých kapilár pro přívod pracovních tekutin ke vzorku a možnosti přívodu potenciálového rozdílu ke vzorku pomocí kapilár vyplněných vodivým materiálem. Dále je v práci prezentován vyvinutý způsob výroby unikátních SNOM hrotů a celý koncept je ověřen provedenými korelativními měřeními. Následně jsou diskutované problémy spojené s výrobou a měřeními.

KLÍČOVÁ SLOVA

SEM, SPM, SNOM, fotonické krystalické vlákno s plným jádrem, proudění plynů

ZEZULKA, Lukáš. *Multifunctional SNOM probes of new generation for correlative SEM/SPM measurements*. Brno, 2021, 55 p. Bachelor's Thesis. Brno University of Technology, Faculty of Mechanical Engineering, Institute of Physical Engineering. Supervised by prof. RNDr. Jiří Spousta, PhD.

DECLARATION

I declare that I have written the Bachelor's Thesis entitled "Multifunctional SNOM probes of new generation for correlative SEM/SPM measurements" independently, under the guidance of the supervisor and using exclusively the technical references and other sources of information cited in the thesis and listed in the comprehensive bibliography at the end of the thesis.

Brno ....

author's signature

ACKNOWLEDGEMENT

First, I would like to thank my family and friends for their persistent support, especially in the harder times.

I am extremely grateful to my supervisor prof. RNDr. Jiří Spousta, PhD, for his kind guidance and mentorship concerning more than just this work. I will always hold his invaluable advice offered to me during the many consultations we had and his joyous view of world in high regard.

I would like to express my gratitude to Bc. Ondrej Černek for all the help he patiently gave me and no fewer for his friendly attitude. My gratitude extends to Ing. Mgr. Tomáš Šamořil, PhD, for his insight regarding the FIB and to Ing. Michal Kvapil, PhD, for his help with the FDTD simulations. Additionally, I would like to thank Ing. Jakub Zlámal, PhD, for his extensive help with simulations, although the results of our cooperation are not explicitly presented in this work.

CzechNanoLab project LM2018110 funded by MEYS CR is gratefully acknowledged for the financial support of the sample fabrication at CEITEC Nano Research Infrastructure.

I am also thankful to the Technology Agency of the Czech Republic (TACR) for the funding received within the project number FW03010504 — Development of in-situ techniques for characterization of materials and nanostructures.

Lukáš Zezulka

Contents

Introduction

The broad ambition of mankind in the field of exploring and researching the world and its true essence knows no limits. Whether talking about lifting the veil of the unknown, laying the furthest away, or quite the opposite, looking into the smallest details all around us. The only prevailing boundaries restraining our advance dwell in the means of research available to those keen on advancing ahead. Past pioneers of their respective fields could not have possibly imagined nowadays methods, instruments, and resources accessible by virtue of their deeds to enjoy the use of.

In this day and age, it is possible to study the world around us on a scale unimaginable in times not so long ago. Scientists around the globe are capable of viewing the structure of surfaces atom by atom. In the year 1942, Zworykin developed *Scanning Electron Microscope* (SEM) and overcame the resolution limit induced by visible light diffraction [1]. Binnig and Rohrer in 1982 contributed to a large extent to these efforts by inventing *Scanning Tunneling Microscope* (STM), first of the several following *Scanning Probe Microscopy* (SPM) techniques[1] [2]. Simultaneous application of these techniques leads to a faster and more detailed reviewing of samples while yielding more pieces of information. Right in this sphere of application, we would like this work to contribute to the endeavour to push the limiting boundaries further away, if not at least outline the possible directions of doing so.

AFM microscope LiteScope$^{\text{TM}}$ developed by NenoVision s.r.o., when installed in an SEM makes it possible to perform correlative SEM/SPM[2] measurements. Our goal in this work is to design a suitable probe for application in these correlative measurements. Furthermore, the design of the probe should be compatible with the enhanced functionalities, which we would like to introduce in the future. Multifunctional probe like this would enable different kinds of measuring, altering, or even creating nanostructures in situ of SEM. With these applications in mind, we explore the possibilities of introducing light, working fluids and potential difference to the area of the sample in close proximity to the probe tip. Nevertheless, our main focus remains on the preparation of the probe in its basic variant for the correlative measurements.

[1] Four years later Binnig, Quate, and Gerber presented derivative method *Atomic Force Microscopy* (AFM) [3].

[2] Alternatively called *Correlative Probe and Electron Microscopy* (CPEM$^{\text{TM}}$) [4].

1 Theoretical part

We performed research on the individual aspects of the preparation of the desired multifunctional SNOM probe as it is depicted later in this work (see figure 3.1 on page 36). We follow up on the previous achievements of Ing. Juraj Bobek and Bc. Ondrej Černek in their master and bachelor theses, respectively [5, 6].

In the first section, we deal with the issue of using *Solid-Core Photonic Crystal Fibre* (SC-PCF) in *Scanning Near-field Optical Microscopy* (SNOM) techniques and we note the results of our research in this field.

The following section concerns the applications of SC-PCF for the introduction of working fluids to the probe tip. We start with a brief theoretical description of the gas flows in capillaries, followed up with a possible single capillary inlet. At the end of this part, we focus on currently available solutions suitable for the introduction of working fluids to the sample.

Last but not least we explore the possibilities of the electrical potential contacts via capillaries filled with suitable material.

1.1 Applications of SC-PCF in SNOM

Abbe's diffraction limit for the resolution of optical systems has been surpassed by far-field techniques, e.g., fluorescence microscopy and near-field techniques such as STM and SNOM [7]. SNOMs avoid the diffraction limit by working in a subwavelength tip to surface proximity, which is dominated by an evanescent field [8].

Near-field optical microscopy, as well as the used tips, can be divided into two categories. First, an apertureless tip, which acts like an antenna and scatters near-field light emitted from an externally illuminated surface. The second is a tip with an aperture, which is brought into focus in this work [9].

In the aperture SNOM regime, the probe converts the emitted near-field light to far-field radiation, which is coupled into the fibre. This is usually considered to be mediated by induced dipoles at the tip. The efficiency of the probe is highly dependent on the properties of the tip and the aperture [10]. Coupled light is to be used for sub-diffraction limit imaging or spectroscopy [9].

Light guidance in SC-PCF is achieved by the modified total internal reflection, which describes the effect of cladding with the microstructured region. The microstructured region consists of air holes in a multilayer hexagonal layout, shown in figure 2.1. Thus, the effective refractive index of the cladding is lower than the refractive index of the core and light is similarly confined in a core as in solid-core fibres, where total internal reflection occurs [11, 12]. Light propagates in an endless single-mode, ergo light propagates only with one reflective angle [13].

1.1.1 Tip fabrication

We focused on the possibility of creating a tip suitable for the SNOM application on an SC-PCF as such. The outcome of our research was divided into three branches based on different approaches. Either fabrication from the fibre itself, using the fibre as a base and creating the tip on top of it or adding an existing tip to the fibre.

Due to the internal structure of the fibre, it is hard to directly apply the conventional methods of tip fabrication used on conventional fibres. The traditional etching techniques, Turner method [14], tube etching [15], meniscus etching [16] are generally problematic because of the capillary actions, which lead to etching from the inside producing unsuitable tips for our purposes [12].

Top-down

Based on the conventional "sealed-tube etching" [17], Christine A. Carlson and Jörg C. Woehl derived a method suitable for SC-PCF as described in their article [12].

The core of this technique is the permeation of 40% HF through a polymer coating while protecting the capillaries with non-permeable sealing. The etching process progresses from the outer rim to the centre, exposing capillaries in the process, which leads to the vertical etching. By etching with a protective oil cover on the surface in an environment with controlled temperature, they were successful in preparing a central tip. It is necessary to immediately dissolve the polymer coating and immerse the fibre into the water to prevent any consequential etching.

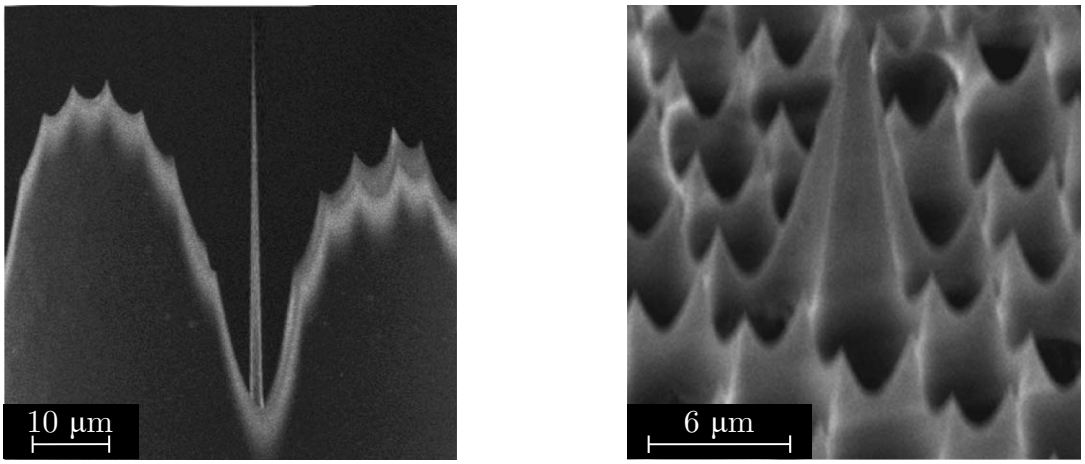

(a) Side-view of an etched tip.

(b) Close-up on central tip surrounded with secondary tips.

Fig. 1.1: SEMs of tip resulting from etching. Adapted and edited from [12].

This leads to the creation of a central tip with a hexagonal cross-section matching

the core size. The air hole structure provides secondary tips. Results are shown in figure 1.1. Tips etched in this way were proven to work as a light source concentrated in the apex.

Bottom-up

Interesting results were achieved by Pura *et al.* with a different approach based on photopolymerization — growing a tip from a photoreactive solution [18].

A drop of the photopolymer liquid is allocated at the end of the fibre with a coupled laser beam. Due to the light-guiding mechanism of SC-PCF, a conic centred tip begins to form. To prevent the photopolymer liquid from pervading into the capillaries, they were prefilled with a different solution with a lower refractive index than silica. The photopolymer presence in capillaries would affect the light-guiding ability of the fibre as a result of its refractive index being higher than that of silica.

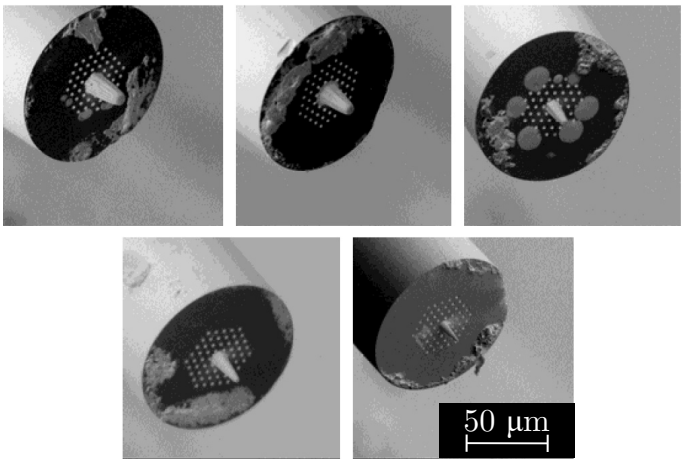

Fig. 1.2: SEMs of the various polymer tips grown with different laser power. From the highest in the top left to the lowest in the bottom right. Adapted and edited from [18].

The dimensions of the grown tip are possible to be controlled by adjusting the absorbed energy by the polymer as shown in figure 1.2.

Attachment of an existing SNOM tip

A different approach involving incorporation of a SNOM tip on a top of SC-PCF was successfully performed by Ing. Juraj Bobek in cooperation with Ing. Mgr. Tomáš Šamořil, PhD, [5].

First, an LMA5 SC-PCF was etched to a smaller diameter (approximately 45 µm), while still preserving the internal capillary structure unmodified. This was achieved

by etching the stripped fibre from the side and later cutting in half. The process continued with a covering the fibre with Au layer in the Kaufman deposition chamber.

To obtain a solid tip, a conventional SNOM probe was made. The conventional fibre was etched applying the Turner HF etching method [14] and the probe was finished with the procedure described in Ing. Petr Dvořák's, PhD, dissertation thesis [19].

The golden layer in the central core of the SC-PCF was removed using FIB. SemGlu, an adhesive hardened with an electron beam [20], was applied onto the uncovered fibre surface.

Using an SEM Tescan LYRA3 equipped with FIB, a nanomanipulator [21] and *Gas Injection System* (GIS) allowed for a successful cut-off and transfer of the tip from the conventionally created SNOM probe. The separation of the tip of the SNOM probe is shown in figure 1.3 and the attachment of the tip to the fibre is shown in figure 1.4a.

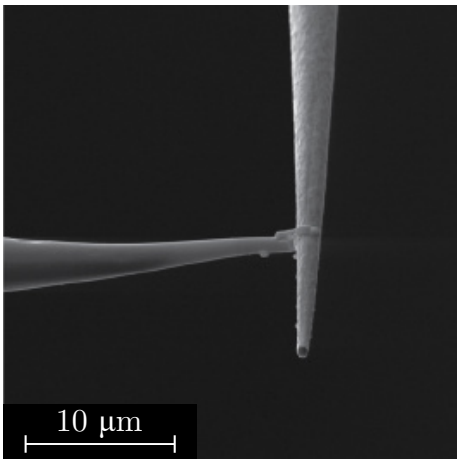

(a) Nanomanipulator attached to the SNOM probe.

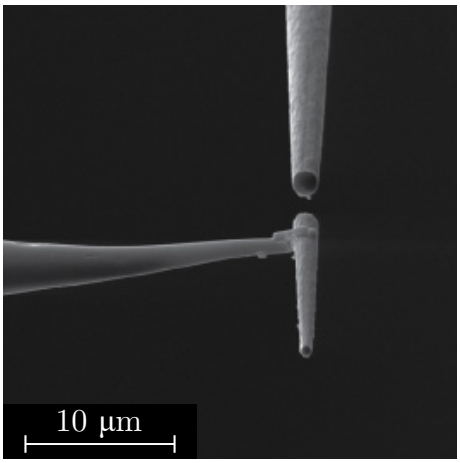

(b) Cut off tip.

Fig. 1.3: SEMs of the tip extraction from the conventional SNOM probe. Adapted and edited from [5].

The excessive surface with the golden layer etched off was covered with a Pt layer, excluding the area of the deposition shadow of the added tip. The result is shown in figure 1.4b. Covering the bare fibre core should prevent light from escaping through this area.

Light coupling to the glued tip was successfully confirmed, but no further measurements were successfully conducted with the created probe because of high lateral forces acting on the glued tip during the shear mode topography measurements.

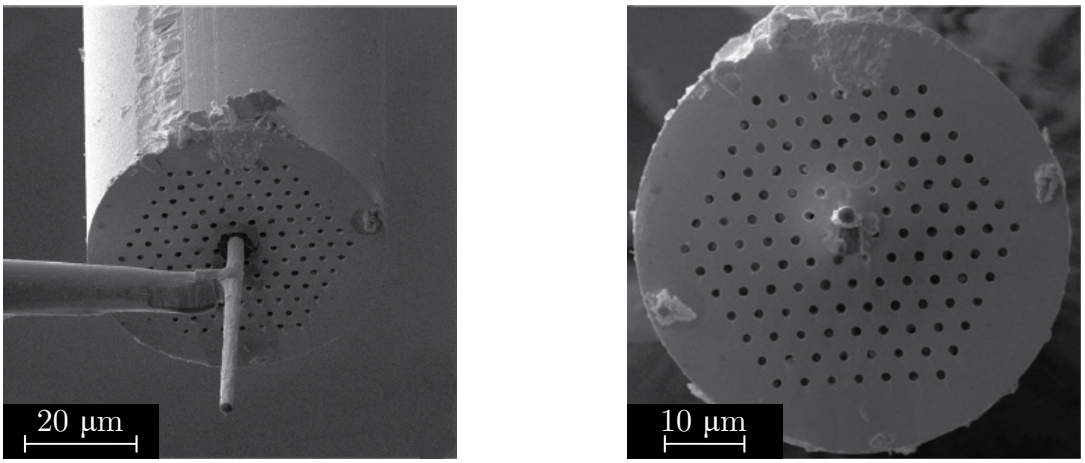

(a) Placing the SNOM tip on the SemGlu with a nanomanipulator.

(b) Attached tip with the surrounding Pt layer.

Fig. 1.4: SEMs of the tip placement from conventional SNOM probe on top of the SC-PCF. Adapted and edited from [5].

1.2 Introduction of working fluids with SC-PCF

Our intention behind using hollow optical fibre for the introduction of working fluids to the sample is the creation of a GIS, which essentially serves for a local chemical deposition. This injection system introduces a chemical precursor[1] to the sample [22].

The implementation into the vacuum chamber of an SEM would allow manufacturing of nanostructures with the *Focused Electron Beam Induced Deposition* (FEBID) technique. The electron beam introduces *Backscattered Electrons* (BSE) to the sample and generates *Secondary Electrons* (SE) in the area where *Primary Electrons* (PE) impact. These electrons create a layer of the deposited material on the surface covered with the precursor [23].

Typically, a capillary with a diameter of 500 µm is used for the introduction of the precursor [23]. The hollow fibres we are interested in using have capillaries with the diameter ranging in units of µm. Fluid flow in such a narrow channel is heavily restricted and many articles are describing it. We will address these later.

1.2.1 Theory of macro-flows

Gas flow in a narrow channel is a trivial problem to study the flow through a hollow optical fibre and to determine a filling time and other properties of a device utilising

[1] Chemical substance transporting substances into a chemical reaction or entering the reaction rising to another substance.

such fibre for the gas flow.

Pressure driven gas flow in capillaries depends on the degree of rarefaction, which is quantified by the Knudsen number. The Knudsen number defines a character of the flow[2] (figure 1.5) and is defined as a ratio of the mean free path (λ) and the characteristic dimension of the flow domain (ℓ):

$$\mathrm{Kn} = \frac{\lambda}{\ell}. \tag{1.1}$$

In the case of the flow in the capillary, ℓ is the diameter of the capillary.

Mean free path is

$$\lambda = \frac{\mathrm{k_B}T}{\sqrt{2}\pi \mathrm{d}^2 p}, \tag{1.2}$$

where $\mathrm{k_B}$ is the Boltzmann constant, T the thermodynamic temperature, d the effective cross-sectional area of a molecule and p the pressure. The combination of equations 1.1 and 1.2 leads to a conclusion that the character of the pressure-driven flow is dependent on the pressure throughout the capillary [25].

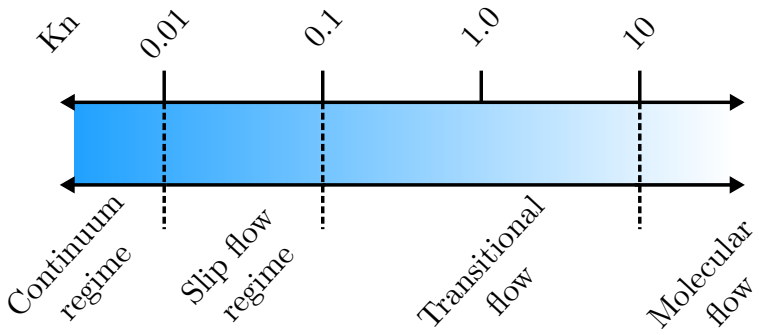

Fig. 1.5: Flow regimes defined by the Knudsen number. Illustrated in Inkscape. Based on [26].

The continuum regime is described by the Navier-Stokes equations with *no-slip* boundary condition. Due to the viscous flow in this regime, the velocity profile in the channel is parabolic with the maximum on the axis of the body and the minimum on the walls. As the mean free path of the molecules is considerably smaller than the characteristic dimension, collisions between molecules are more important than collisions with walls [27, 28].

In the slip flow regime, the *no-slip* boundary condition fails because on the outer rim of the channel a layer with different dominant flow forms. This layer covering the

[2]Boundaries between regimes are not strictly given and one can find sources with different ranges, e.g. [24].

walls is thick about one mean free path. The flow in such a layer can be neglected by introducing a non-zero velocity on the boundary. Hence, the gas slips on the walls and the regime is called the slip flow. Computation of an isothermal slip flow is possible by the Navier-Stokes equations with a first order Maxwell's velocity slip boundary condition. Collisions between molecules still prevail [26].

Transitional regime describes the flow transforming its characteristics from the continuum to the molecular flow. The flow in this regime is described by the Boltzmann equation[3] or models with higher-order corrections. To avoid a complicated solution of the Boltzmann equation, *Direct Simulation Monte Carlo* (DSMC)[4] is introduced [26, 29, 30]. The minimum flow rate has been experimentally found in this regime at Kn ≈ 1. Collisions with walls and mutual collisions are equally important [31].

In the molecular flow, often called free molecular flow, a high degree of gas rarefaction leads to a change in the character of molecular collisions. The molecules no longer bounce off each other, instead, they are more likely to collide with walls. Thus, this flow is described with the collisionless Boltzmann equation and can be possibly simulated using the DSMC [32].

1.2.2 Gas flow in photonic crystal fibres

Hollow optical fibres are used to create gas concentration sensors based on the interaction between light and gas molecules in the fibre [33, 34]. The filling time and the dynamics of the flow are crucial parameters when designing such a sensor and have been thoroughly studied [35, 36, 37].

Parman and Bhatnagar in their article "Analysis of gas flow dynamics in hollow core photonic crystal fibre based gas cell" presented a model for estimating the filling time of a core and cladding holes in a *Hollow-Core Photonic Crystal Fibre* (HC-PCF) with gas [38].

Their model is based on computing the change in pressure along the fibre and an appropriate diffusion coefficient to evaluate the filling time. The considered HC-PCF (HC-1550-02) sold by NKT Photonics (figure 1.6) has a 10.4 µm core diameter and a 3 µm diameter of cladding holes [39]. Acquired filling times as a function of the fibre length are depicted in figure 1.7 for two filling pressures. The filling time was found to increase with the length of the fibre and decrease with the diameter of the capillary.

[3] Boltzmann equation stands valid in the whole region of Knudsen flows, but easier descriptions are available [29].

[4] DSMC is also usable in the whole region of Knudsen flows.

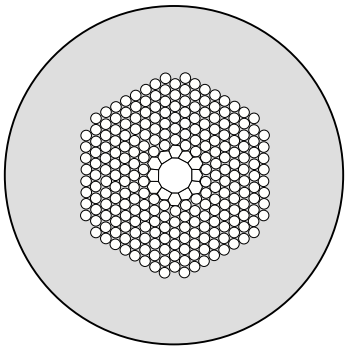

Fig. 1.6: Schematic of the HC-PCF, HC-1550-02 sold by NKT Photonics with a 10.4 µm core diameter and a 3 µm diameter of cladding holes. Adapted and edited from [39].

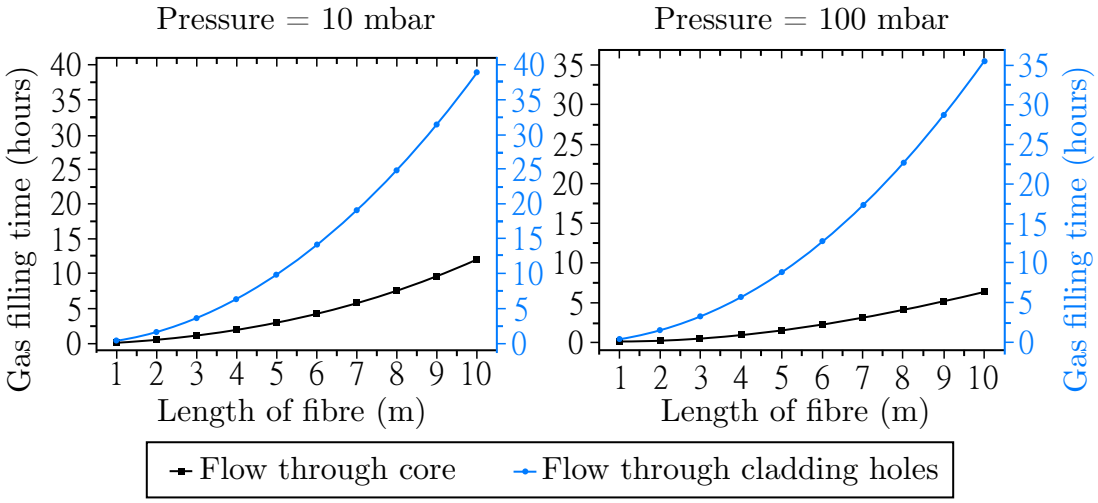

Fig. 1.7: Filling times for acetylene gas in both the core and the cladding holes in HC-PCF for two ambient pressures. Adapted and edited from [38].

Furthermore, they established that with an increase in the ambient pressure, the filling time lowered and filling with more viscous gas takes longer.

1.2.3 Single capillary inlet

Our goal in this section is to theoretically explore the possibilities of creating a localised gas source close to the apex of the tip. A way to achieve this is by introducing the gas only through a selected capillary with an outlet in the desired area. We divided the proposed solutions into two different branches.

Direct capillary inlet

We put forward the creation of an inlet into the capillary on a cleaved end of the fibre. First, the face of the microstructured region of the fibre would have to be covered with a layer of material. Subsequently, an inlet to the selected capillary would be created in this sealing mask using, for example, the FIB technique.

This approach brings problems with light coupling into the core. The mask would either have to be light-permeable or etched off from the core in the same manner as in the case of the capillary inlet.

Alternatively, a material with a lower refractive index than silica could be introduced into the air channels and consequently an aperture into one of the capillaries could be created with FIB.

The end of the fibre with this inlet would be placed in a pressurised chamber, where another optical fibre would have to be introduced to provide light coupling to the SC-PCF.

Lateral capillary inlet

Hensley *et al.* in [40] and Brakel *et al.* in [41] presented a method for creating lateral microchannels in the optical fibre using femtosecond laser pulses as shown in figure 1.8. Both mentioned articles focus on creating gas cells in hollow optical fibres.

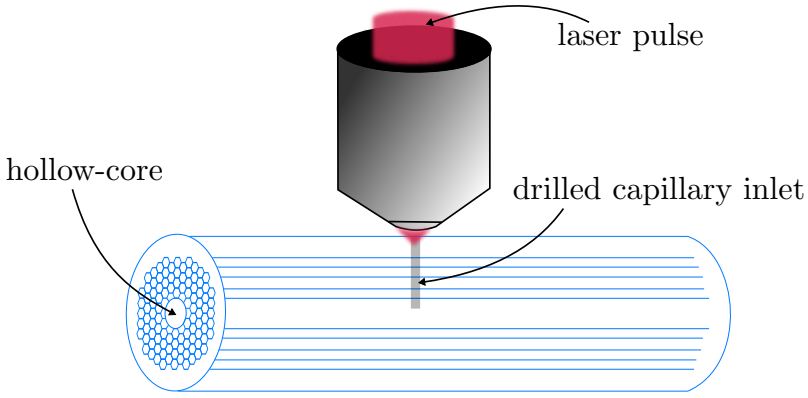

Fig. 1.8: Experimental setup for micromachining the channel with laser. Adapted and edited from [40].

Hensley *et al.* managed to drill a channel with a surface diameter of 1.5 µm, which caused a loss of 0.35 dB (about 7.74 %) and is shown in figure 1.9. This inlet was capable of filling the core of a used HC-PCF with gas.

Brakel *et al.* were able to drill an inlet into an SC-PCF resulting in a loss of 0.5 dB (about 10.9 %) and into an HC-PCF with a surface diameter of 20 µm, which

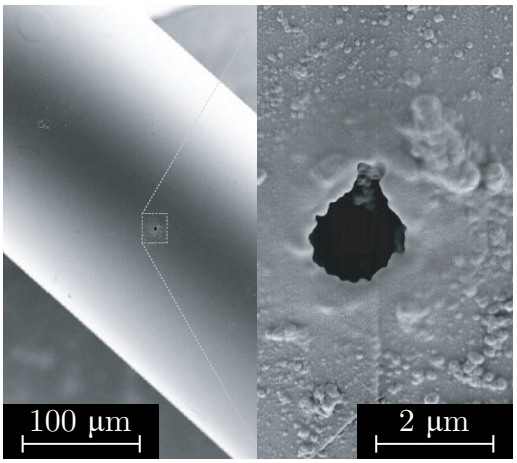

Fig. 1.9: SEMs of the HC-PCF with the drilled inlet. Adapted and edited from [40].

did not lead to a loss in transitivity. The section of the drilled inlet into both fibres is show in figure 1.10. Acetylene diffusion through the inlet was successfully confirmed in the case of HC-PCF.

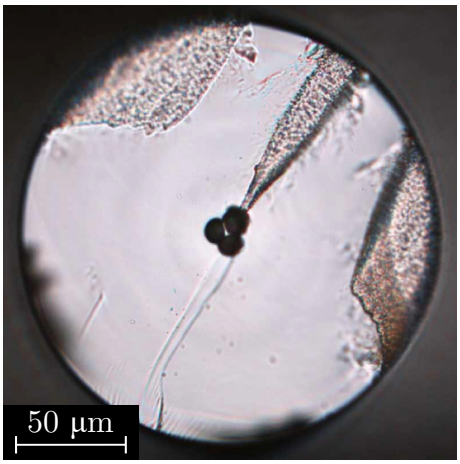

(a) Optical image of inlet drilled into the SC-PCF.

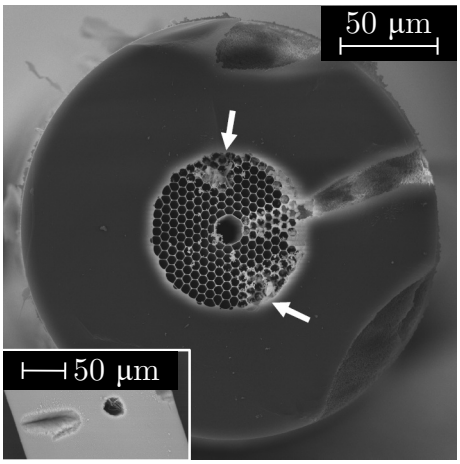

(b) SEM of an inlet drilled into an HC-PCF.

Fig. 1.10: Created lateral capillary inlet. Adapted and edited from [41].

1.2.4 Available alternative

FluidFM® made by CYTOSURGE is a commercially available SPM probe capable of introducing working fluids to the sample. The cantilever of the probe is hollow and the outlet of the microchannel is positioned close to the tip (figure 1.11)[42].

The company offers two different probes with a pyramidal tip, which differ in the size and position of the outlet. FluidFM® nanosyringe with a 600 nm side aperture

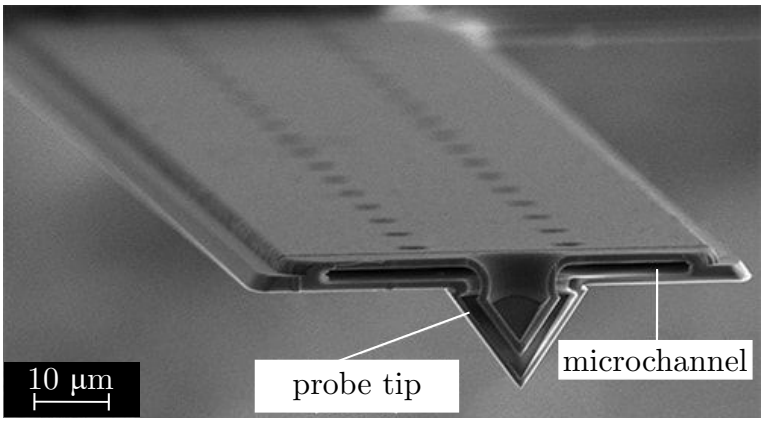

Fig. 1.11: SEM of the cross-section of the probe showing the microchannel leading to the tip. Adapted and edited from [42].

and FluidFM® nanopipette with a 300 nm top aperture are shown in figure 1.12. Both of these are suitable for nanoprinting.

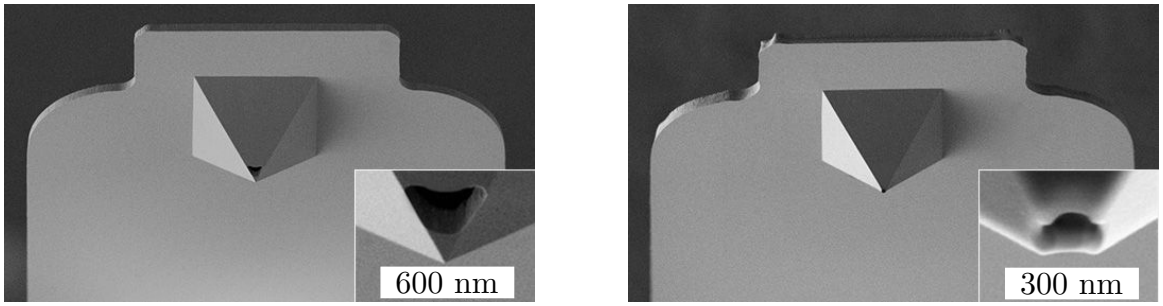

(a) FluidFM® nanosyringe.

(b) FluidFM® nanopipette.

Fig. 1.12: SEMs of the FluidFM® probes. Adapted and edited from [42].

Souza *et al.* in their article "Three-Dimensional Nanoprinting via Direct Delivery" utilized the FluidFM® nanopipette for nanoprinting. A photopolymer hardened with UV light was used as the printing material. They were able to carry out printing with 6 ± 1 nm precision in all axes [43]. Their results are shown in figure 1.13.

1.3 Capillary wires

Capillaries filled with a conductive material would provide suitable electrodes which could be used to bring an electrical potential difference to the close surroundings of the tip. The microstructured region with only a few capillaries filled should not be

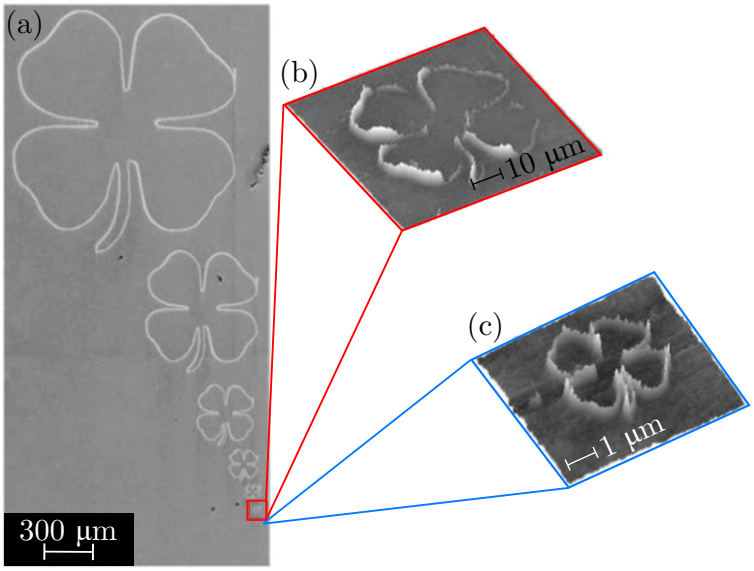

Fig. 1.13: (a) SEM of the clovers printed with the FluidFM® probe in seven different sizes. (b) 3D AFM topography of the sixth clover (red square in the (a)). (c) 3D AFM topography of the smallest clover (blue square in the (a)). Adapted and edited from [43].

altered too heavily and light guidance is expected to be approximately preserved. We refer to these as the capillary wires.

We aim to theoretically explore methods of creating capillary wires suitable for our cause. The subject of consequential interest beyond the scope of this work would be whether the capillary wires do not alter the resonant frequency of the probe too much and whether they work without cracking.

1.3.1 Golden wires

Lee *et al.* in the article "Pressure-assisted melt-filling and optical characterization of Au nano-wires in microstructured fibers" [44] describe a splice filling technique, which led to successful creation of a golden capillary wire in one selected air channel.

Capillaries with various diameters ranging from 120 nm to 2 µm and just about 10 cm long were filled. The ones with a diameter larger than 1.2 µm were able to sustain unbroken wires several centimetres long and were proven to be conductive.

First, a capillary with a large inner diameter containing a golden wire was joined to the SC-PCF (or to a *Modified Step Index Fiber* (MSIF) with a hollow channel running parallel to a doped core). Additionally, a middle section could be introduced for selective filling. This was achieved by splicing a capillary with an eccentric

channel in between the capillary with golden wire and the SC-PCF. Eventually, this setup was brought into a vertical furnace and heated up to ~1064 °C and at this point argon at a pressure of several hundred bars was introduced. This drew the melted gold into the uncovered capillaries. The described procedure and achieved results are depicted in figure 1.14.

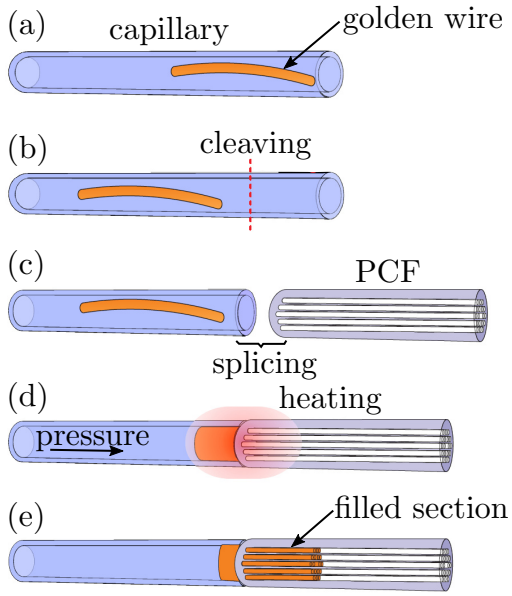

(a) Schematic of capillary filling with gold.

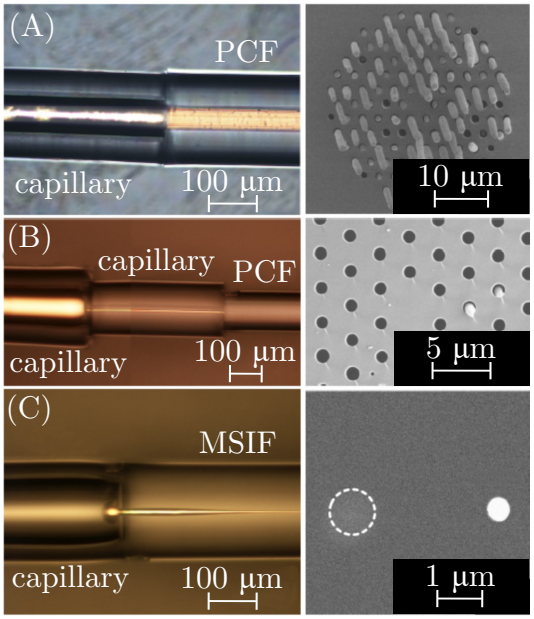

(b) Optical side-view and SEMs of the ending. (A) Capillary wires in every capillary. (B,C) Selective filling.

Fig. 1.14: Golden wires inside of the SC-PCF, the manufacturing mechanism and the results. Adapted and edited from [44].

1.3.2 Liquid metal wires

To avoid cracking of the wires in stretchable electronics, metals that are liquid at about room temperature are used [45, 46], e.g., gallium with a melting point at 29.7646 °C [47] and its alloys.

In the article "Vacuum filling of complex microchannels with liquid metal" Lin *et al.* presented an available and easy to apply procedure of filling channels with a liquid metal [48].

Microchannel structure created in *poly(dimethylsiloxane)* (PDMS) with a single punched inlet covered with EGaIn (Eutectic Gallium-Indium) drop was placed in a vacuum with base pressure ~6.5 kPa for ~20 minutes. While in a vacuum, the air trapped in the channels is forced to bubble through the drop by the pressure

difference, which seals the inlet. After returning to the atmospheric pressure, the pressure difference pushes the liquid metal into the air channels (see figure 1.15a). PDMS is capable of absorbing a nonnegligible amount of residual gas trapped in the channels, this further supports the filling.

The presented process was capable of creating wires with diameters as small as few microns. Performing a test on a tapered channel led to the partial filling which terminated at a width of approximately 5 µm as shown in figure 1.15b.

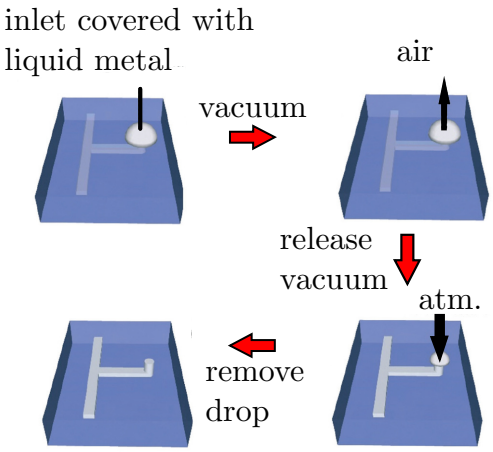

(a) Schematic of the capillary filling with liquid metal.

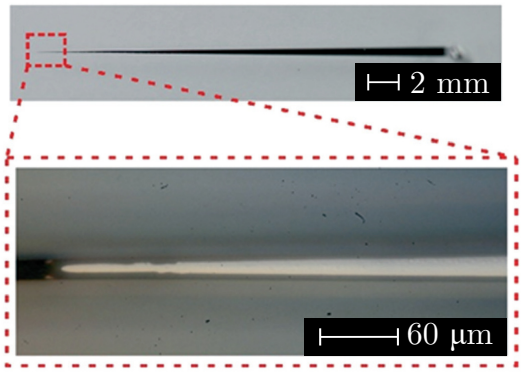

(b) Optical view of the partially filled tapered channel.

Fig. 1.15: Liquid metal channel filling. Adapted and edited from [48].

The minimal achieved channel width that was still filled is not sufficient for our purposes, although this process has the potential to be altered. Placing the sample into a considerably higher vacuum for a longer time and using liquid metal with lower surface tension might lead to better performance. Moreover, the article deals exclusively with single inlet problematic, we propose that both ends of the fibre could be covered with a single drop. Furthermore, to create wires only in the selected capillaries, a selection mask would have to be introduced as well.

2 Unique tip designs and FDTD simulations

Our goal in this section is to design various fibre tips and use Lumerical *Finite-Difference Time-Domain* (FDTD) simulation software to evaluate their capability of light guidance. Furthermore to decide if the tip apex can be considered as a light source in the near-field.

We aim to design tips with the apex close to one of the capillaries in the fibre. This would potentially provide a source of light (aperture in the apex) and working fluid (capillary outlet) close to each other.

2.1 Fibre model

Prior to the tip modelling process, we created a whole and unmodified model of the fibre we planned to use — LMA-5 [49] — shown in figure 2.1. The blueprint of the fibre is based on the geometry measurements listed in table 2.1.

Tab. 2.1: Important measures of the LMA-5 optical fibre.

core diameter	5 µm
cladding diameter	125 µm
coating diameter	245 µm
capillary diameter	1.276 µm
capillary pitch	2.9 µm

Note: Core, cladding and coating diameter data are accessible directly from NKT Photonics [49]. Capillary diameter and pitch available from OPTICS EXPRESS article [50].

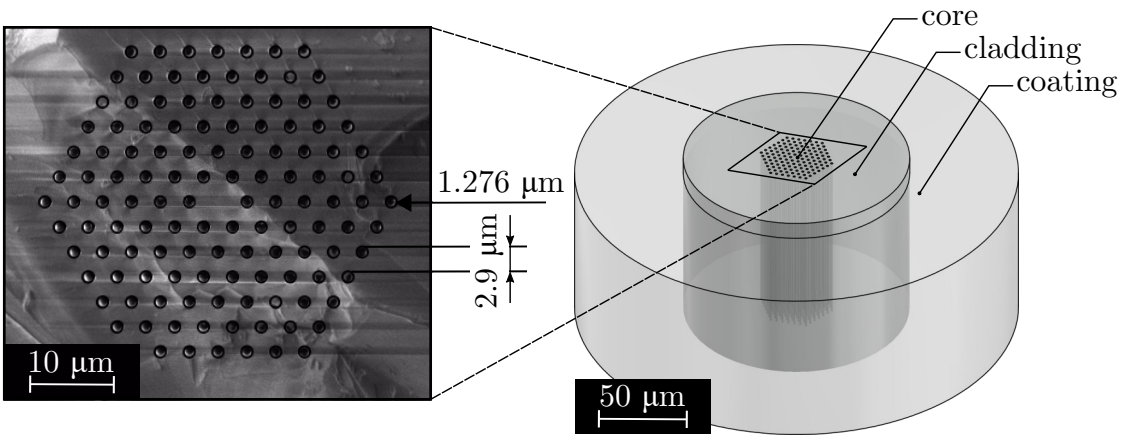

Fig. 2.1: Model of the LMA-5 optical fibre and detail of the microstructure region layout overlayed with SEM (Tescan LYRA3). Created using Inventor and Inkscape.

2.2 Tip designs and modelling

In the process of the tip design creation, one of our primary concerns was the ease of fabrication using the FIB technique. All designs were drafted with a need for a view from three specific angles via FIB. Two side views which are mutually perpendicular for the body fabrication and a top view for milling the aperture.

Our first design is shown in figure 2.2 and from now on we will refer to it as the "obelisk tip". The base of the tip is rectangular and the apex with the aperture is located in the core region but shifted towards a capillary in the inner layer.

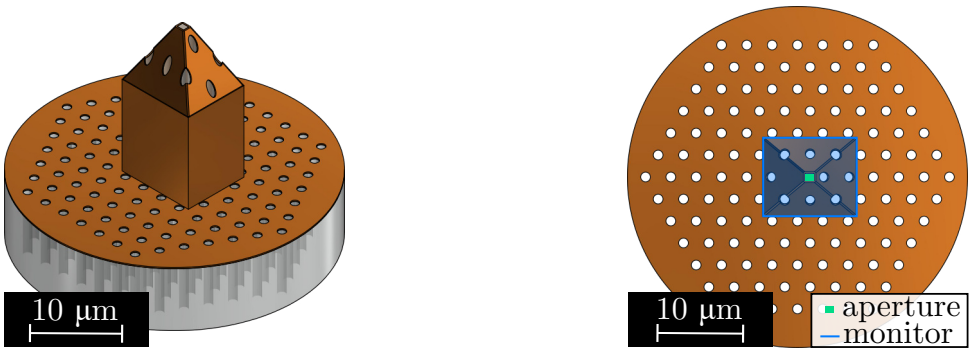

(a) 3D view. (b) Top view.

Fig. 2.2: Obelisk tip. Created in Inventor.

Our next design was derived from the obelisk tip and is called the "pyramidal tip" (figure 2.3). The apex and the aperture are positioned in the same way as in the previous design, but the extra mass on the sides of the tip body could enhance the rigidity and the firmness of the tip.

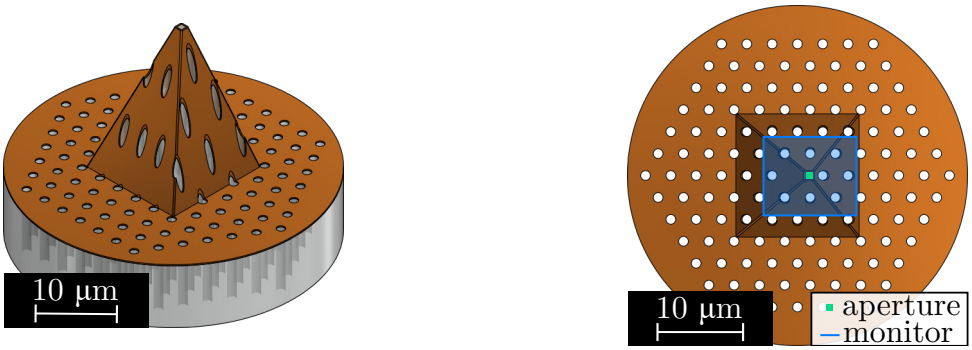

(a) 3D view. (b) Top view.

Fig. 2.3: Pyramidal tip. Created in Inventor.

The last presented design (figure 2.4) features an apex with an aperture in the outer rim of the microstructured region and thus is called the "eccentric tip". We

consider this design advantageous for the possible creation of a side inlet into the capillary in the outer rim of the microstructured region, as described in section 1.2.3, with minimal destruction of the inner structure. The drawback of the high eccentricity of the aperture is expected to be a low intensity of the transmitted light.

(a) 3D view.

(b) Top view.

Fig. 2.4: Eccentric tip. Created in Inventor.

We created 3D models of the tips in a ".ipt" format using Autodesk Inventor. Tips were modelled from a narrowed fibre with a diameter expected after the etching in an HF, 45 µm. Based on those models we were able to create fitting models of the outer golden layer[1]. Finally, the created models were exported into ".STL" format, which we were able to import into Lumerical FDTD.

2.3 FDTD simulations

Under the supervision of Ing. Michal Kvapil, PhD, we continued with work in the Lumerical FDTD.

First, we tested the light guidance ability of the tips. A plane wave with a wavelength 532 ± 1 nm and unit electrical intensity was introduced into the end of the fibre and propagated in the fibre for approximately ten wavelengths before reaching the region of the tip.

To lower the computational difficulty of the simulations we created approximately 1 µm large aperture in the golden layer (figure 2.5). The simulation grid with a step of 40 nm was used in all of the three simulations.

The output of these simulations was detected in a monitor placed in the near-field approximately 200 nm from the tip. The operational distance of the tip from the sample is expected to be up to tens of nm [9]. A larger distance still sustaining

[1] Golden layer on the sides of the etched fibre and an adhesive titanium layer were in the models neglected.

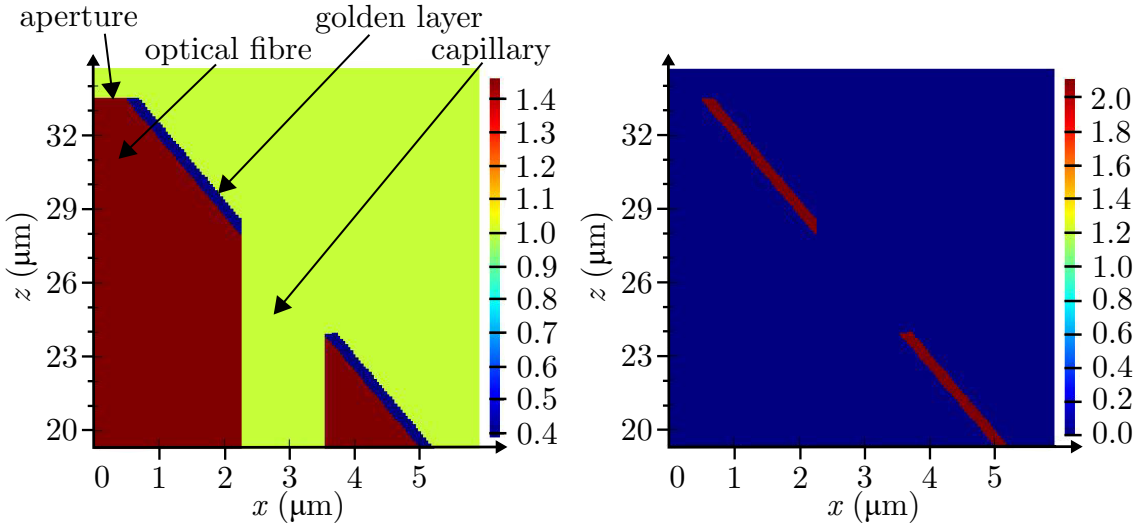

(a) Real part of the refractive index. (b) Imaginary part of the refractive index.

Fig. 2.5: Index preview of the apex with an aperture, pyramidal tip. The model is symmetric in the z axis. Exported from Lumerical FDTD.

near-field condition was chosen, to preserve at least five simulation cells between the aperture and the monitor.

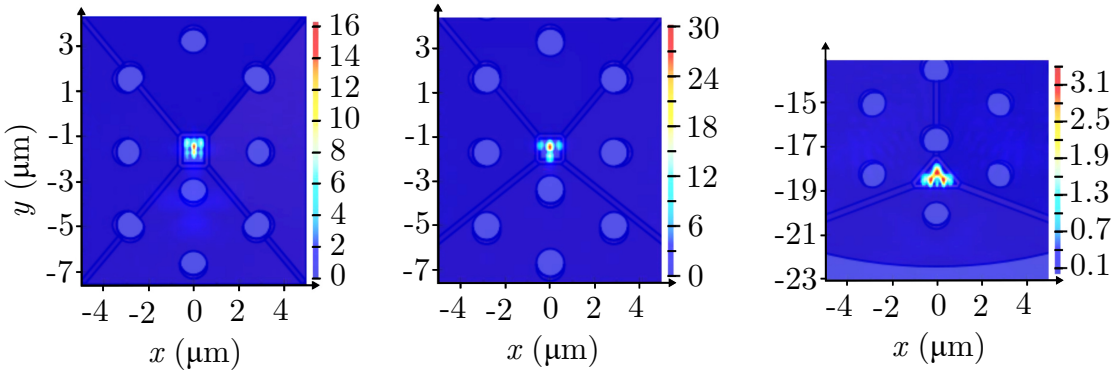

(a) Obelisk tip. (b) Pyramidal tip. (c) Eccentric tip.

Fig. 2.6: Square of the module of the electrical intensity in the near-field from the tip. Overlay with a groundplan of the model. Figures are not scaled equally. Monitor recording output shown in (a), (b), and (c) is marked off in figure 2.2b, 2.3b, and 2.4b, respectively. Exported from Lumerical and edited in Inkscape.

According to our results, shown in figure 2.6, all three designed tips should act as a light source in the near-field. All tips show the capability of localizing the confined light into the desired area. The maximum intensity for the obelisk tip and

the pyramidal tip is roughly comparable. In the case of the eccentric tip, we observe significantly lower maximal intensity, compared to the others.

In this section, we presented three probe tips designed in a way utilizing one of the capillaries as the possible precursor source close to the apex with an aperture. Using FDTD simulations we confirmed the capability of the tips to direct the light confined in the fibre into the desired area. Based on these findings we could roughly assume the tips should be able to perform SNOM measurements as well. The drafted designs will later serve as a basis for the tip fabrication described in section 3.1.2.

3 Multifunctional probe tip fabrication

Our drafted multifunctional probe (see figure 3.1) should be in its basic functionality capable of carrying out correlative SEM/SPM measurements [51] and additionally being capable of introducing light to the sample or performing SNOM measurements (section 2.3). More advanced planned functionalities are an introduction of working fluids to the sample utilizing SC-PCF (section 1.2.2) and bringing the potential difference to the close surroundings of the tip with capillary wires (section 1.3).

In the theoretical part of this work, we explored possible ways of achieving some of the desired functionalities of the probe. From now on, we will focus on the preparation of a tip on an SC-PCF based on the drafted designs in the previous chapter (section 2.2). Other functionalities than the correlative SEM/SPM measurements are taken into account only on a future plan basis.

The proposed probe is based on the concept of an optical fibre glued to a tuning fork in a special manner developed by Bc. Ondrej Černek. We cooperated heavily on the utilisation of an SC-PCF in this approach. The lower rigidity of the hollow fibre compared to fibres with a full-body allows for fabrication and measurements in a tapping mode. The developed technique of fibre gluing makes it possible to fine-tune the resulting resonant frequency by positioning the fibre in a specific form. The utilisation of a hollow optical fibre for SNOM measurements in a tapping mode variant is to our best knowledge and belief a unique and novel approach. This concept is beyond the scope of this work and is a subject of associated research within the framework of TACR project FW03010504 — Development of in-situ techniques for characterization of materials and nanostructures. Shear mode applied in this work is more discussed in section 3.1.3.

3.1 Manufacturing the probe

3.1.1 Fibre etching

Etching the fibre is important for the future modifications of the fibre with FIB milling as the reduced diameter of the fibre leads to shorter milling times. Furthermore, etching reduces the total weight of the fibre glued to the tuning fork. A high load glued onto the tuning fork might negatively affect the oscillations of the probe.

For our purpose of etching an SC-PCF, we developed a new drop etching technique with 40 % *hydrofluoric acid* (HF) (figure 3.2). This technique allows reducing the outer diameter of the fibre without destroying the microstructured region in the fibre cladding. We applied this procedure to a fibre of a total length of 20 cm, see figure 3.4 for the results.

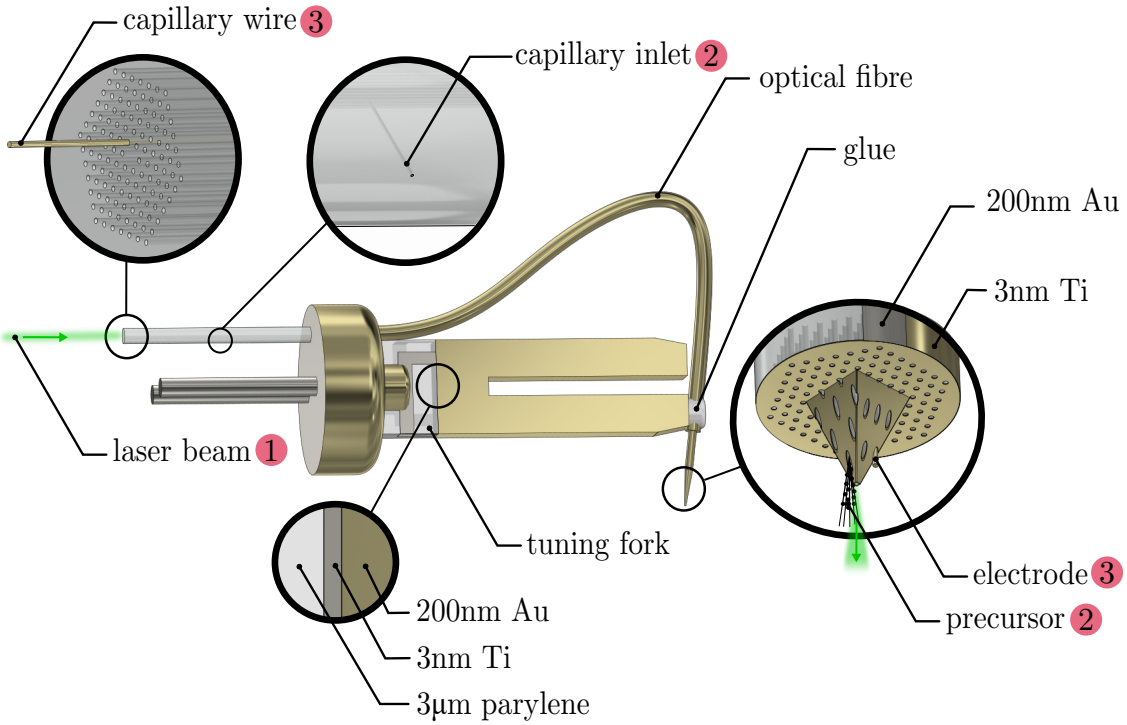

Fig. 3.1: Illustration of the desired multifunctional probe in the tapping mode variant. The unique method of fibre gluing on the tuning fork developed by Bc. Ondrej Černek. Our tip designs for SEM/SPM correlative measurements are reviewed in section 2.2. Advanced functionalities: 1 - light introduction (for the light confinement capability of the proposed tips see figure 2.6), 2 - introduction of working fluids (fabrication of the selective inlet is discussed in section 1.2.3), 3 - capillary wires bringing potential difference (means of fabrication examined in section 1.3). Depicted coating layers are discussed in section 3.1.3. Created in Inventor and Inkscape.

The first step in the process of fibre etching is stripping off the acrylate coating from the approximately 1 cm long middle section. Coating cohesion in this section is reduced by shaving off parts of the coating with a sharp scalpel. This is done by placing the blade perpendicularly to the surface of the coating and while applying a small amount of force, moving the blade along the middle section. Following the preparation step, stripping is finished with the standard stripping tool (figure 3.3a) for optical fibres pliers like hand tool [52].

For the etching itself, the prepared fibre is freely placed onto a Teflon underlay and using a micropipette, 4 to 9 µl of the 40 % HF are poured on the centre of the stripped middle section. The HF drop will slowly dissolve the fibre cladding and vaporize. After the complete vaporization of the liquids, a new drop is poured on the same spot, but before doing so it is possible to check the etching degree of the

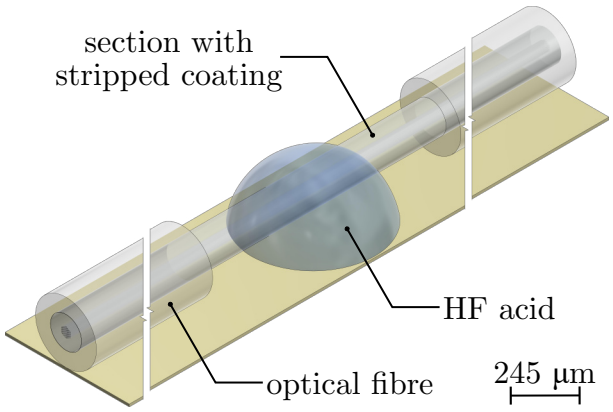

Fig. 3.2: Illustration of the drop etching technique applied on the SC-PCF. Created in Inventor and Inkscape.

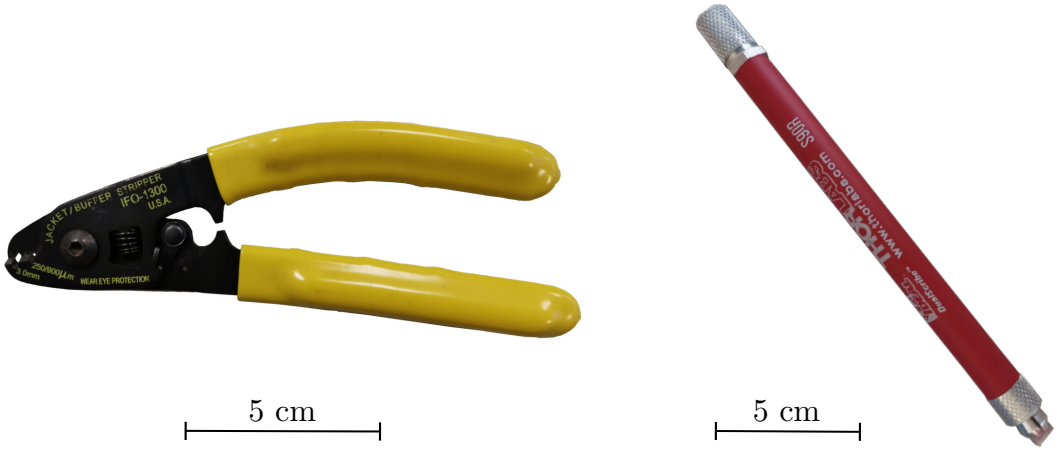

(a) Stripping tool for optical fibres.

(b) Fibre cleaver tool.

Fig. 3.3: Photographs of the stripping tool used to strip down the coating and fibre cleaver tool used to cut the etched fibre.

section with an optical microscope. This provides better control of the process. We observed, that to etch the fibre to the desired diameter (approximately 45 µm), it has to be etched with the drops for about 53 minutes in total. Since the etching speed is dependent on the ambient temperature and the air moisture level, the resulting diameter after the etching varied.

It is crucial for the drop to be placed only on the exposed cladding and to not touch the edge of the coating. This would lead to an under etching of the fibre under the coating.

After the etching, the fibre is cut in the middle section, right where the diameter is the smallest. The cut is carried out with a fibre cleaver tool (figure 3.3b) [53]. This provides us with two etched fibres from every one etching procedure. The cleaved

end is usually imperfect (figure 3.4b), but considering the following FIB milling, this is not considered an issue.

(a) View of the whole stripped section after the cut.

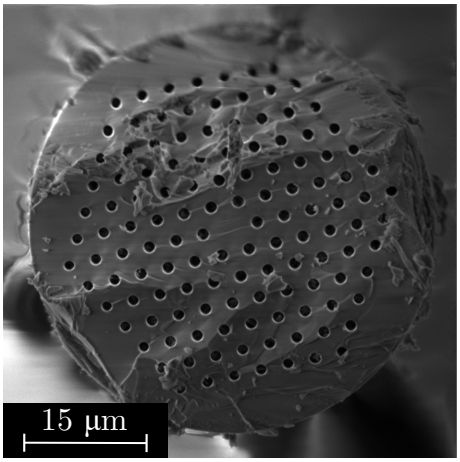

(b) Cross-section of the cut.

Fig. 3.4: SEMS of a fibre etched with the drop technique for 53 minutes. Visible charging of the fibre. Tescan LYRA3.

3.1.2 Tip preparation

For the manufacturing of the tip on the etched fibre, the Tescan LYRA3 dual-beam electron microscope available at the *Central European Institute of Technology* (CEITEC) was used. This microscope combines FIB and SEM and the beams cross at 55°. We used FIB mainly for the milling and SEM for the imagining and to reduce the charging of the fibre during the milling. Stage in this microscope has five degrees of freedom allowing us to move the stage in *xyz*, rotate it around the vertical axis, and pitch it. Furthermore, the chamber of the microscope is equipped with an *Infrared* (IR) camera capturing the stage from a side. Feedback from the camera is important for safe manipulation with the fibre in the chamber. For imaging are available BSE and SE detectors.

We used uncoated fibres to save a step in the manufacturing procedure because we plan to coat the fabricated probe with a golden layer at the end.

FIB milling is the most time-consuming step in the process due to the large volumes that we need to remove to form a suitable tip. To create a rough tip took us about five hours of work. We used a gallium ion beam at 30 keV accelerating voltage and 1.3 nA current for rough milling, 700 pA current for more precise milling, and 1 pA current for imaging. For reviewing the results during the fabrication and for

imaging the final product was used SEM with 5 keV accelerating voltage to lower the undesired charging effect as much as possible.

The fibre holder available at the microscope (figure 3.5), which is used to fabricate conventional SNOM probes [54], is not ideal for our purpose. We need to be able to set the fibre perpendicularly to the ion beam in two positions rotated 90° from each other. Effectively allowing us to view the fibre via the ion beam from two perpendicular sides. The available holder fixes the fibre at an angle of about 45° from the base of the holder and allows us to view the fibre only from one side.

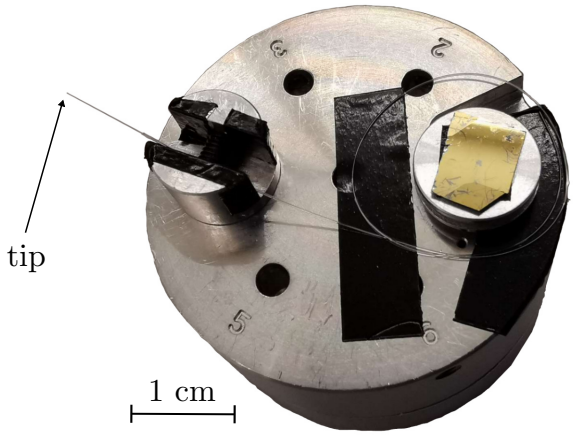

Fig. 3.5: Photograph of the optical fibre in the original holder (left stub) for manipulation in the Tescan LYRA3. On the right stub is a golden plate for fine-tuning the FIB away from the fibre itself.

To overcome this inconvenience, we designed and had made a new holder, which secures the fibre in an upright position. Having the fibre parallel to the axis of rotation of the stage ensures a view of the fibre from different sides (figure 3.7). In our new holder, the fibre is threaded around two screws and secured at the top with carbon tape (see figure 3.6). This way the fibre is firmly held in one position and prevented from drifting.

Using this new holder, it is much easier to position the fibre to view the cross-section of the fibre with SEM as it requires only the movement with the stage in *xyz*. Furthermore, it is also easier to put the fibre in a position, where one can acquire the side views of the fibre with FIB. However, it is not possible to place the fibre perfectly perpendicularly to the ion beam. The negative tilt of the Tescan LYRA3 dual-beam electron microscope is limited to a -30° and the right position would be at a tilt of a -35°. Nevertheless, it is the best positioning we were able to accomplish and suits our purposes well.

For the fabrication itself, we decided to go with the obelisk tip design (figure 2.2), because we considered it the easiest variant to fabricate. We drafted the following

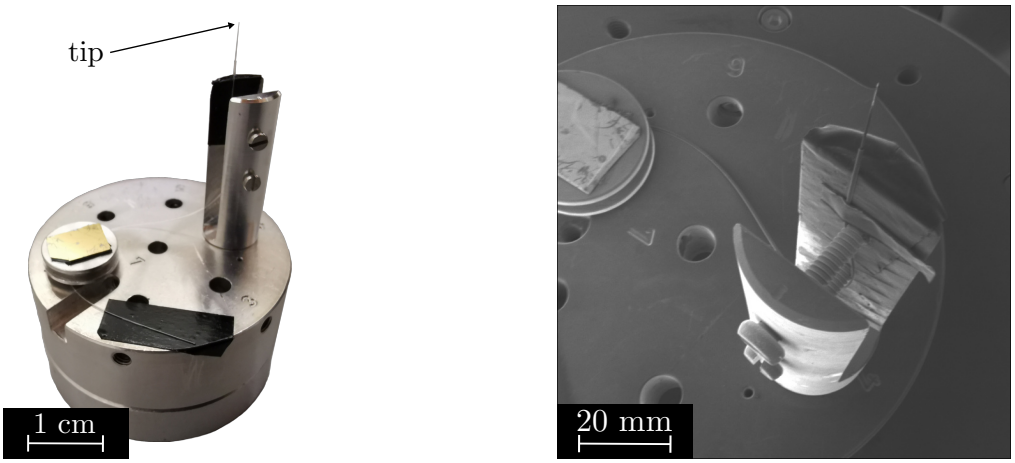

(a) Photograph. (b) SEM. Tescan LYRA3.

Fig. 3.6: New fibre holder (right stub) with the optical fibre secured upright and a stub with a golden plate mounted on the carousel stage.

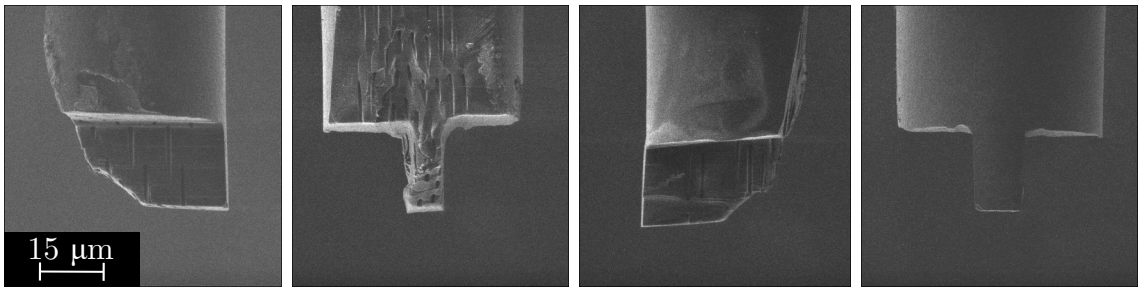

Fig. 3.7: Demonstration of the full rotation capability of an almost perpendicularly positioned fibre to the ion beam. For the demonstration was chosen fibre modified with FIB. The rotation step is 90°. Images were acquired with Tescan LYRA3 FIB.

several-step methodology for fabricating the obelisk tip. First, we would check the diameter of the etched fibre with SEM. For this purpose, we would place the fibre in a position, where we would be able to make an image of the cross-section of the fibre. The stage with a new holder in this position is shown in figure 3.8a. We would proceed to the FIB milling with fibres etched to a diameter smaller than 50 µm and larger than 42 µm. These diameters approximately correspond to fibres etched up to the internal microstructure region with toleration of the exposed outer capillaries.

The fabrication of the central column for the obelisk tip was to be done in the position where FIB scans the fibre from a side. What the stage in this position looks like in the chamber view, is pictured in figure 3.8b. We projected the two-step milling of material from two sides of the fibre leaving us with a ridge in the centre (figure 3.9 step (a)). Areas to be removed would be milled with the rough milling setup and their size would be adjusted in a way to make the ridge at least 15 µm

tall and 10 µm wide in the middle, where the core is located.

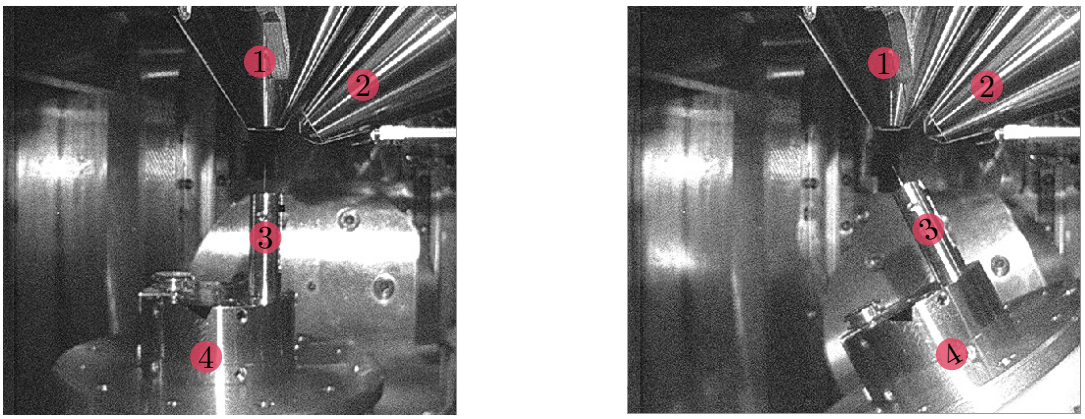

(a) Top view of the fibre with SEM.

(b) Side view of the fibre with FIB.

Fig. 3.8: Chamber view with the IR camera in the Tescan LYRA3 (1 - SEM objective, 2 - FIB objective, 3 - new fibre holder, 4 - stage with 5 degrees of freedom). The stage is captured in two key positions.

Following up on the successful creation of the ridge on the fibre, we would proceed with the fabrication of the central column. To see the ridge from a side with FIB, we would have to rotate the fibre for 90° (figure 3.9 step (b)). In this orientation of the fibre, we should have been able to mill the outer parts of the ridge leaving us with the central column (figure 3.9 steps (c) and (d)). This was expected to be tricky because we desired to preserve at least one capillary in the column.

After the successful fabrication of the central column featuring a capillary in its volume, we aimed to fabricate the apex of the tip. For milling the apex out of the pillar, the precise milling setup was chosen. With the utilisation of this FIB setup, the pyramidal shape would be fabricated from the top part of the sticking-up column. Taking advantage of the freedom in the rotation of the fibre, a precise location for the apex close to the capillary outlet could be selected. Performing this process would create the obelisk tip according to the design depicted in figure 2.2.

The first tip, we somewhat successfully created following along the described fabrication process, yet with the fibre placed in the original holder, is shown in figure 3.10. This tip was fabricated on a fibre etched for too long resulting in exposing the six outermost capillaries. Due to the inconvenient manipulation with the fibre using the old stub, we were not able to keep to the described steps perfectly. We performed milling in imperfect positions and as a result, the obelisk and its surroundings were not properly shaped. We did not manage to fabricate the apex close to an outlet

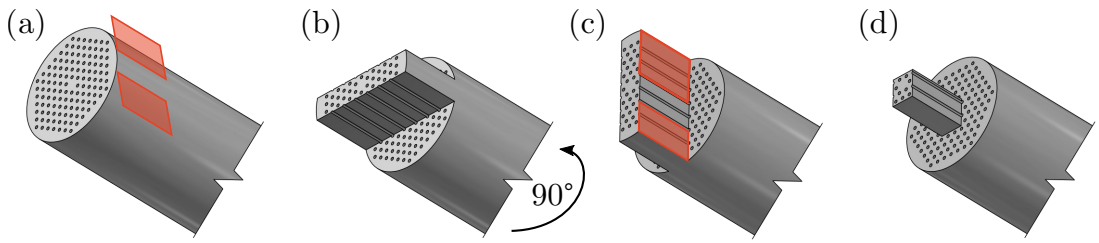

Fig. 3.9: Schematic of the obelisk tip fabrication on an SC-PCF with FIB milling. The process puts in practice rotation capability of the new holder demonstrated in figure 3.7. The red rectangles in the schematic represent areas milled with FIB. (a) Milling sides of the fibre. (b) Rotation of the fibre for 90°. (c) Asymmetrical milling of the ridge. (d) Central column resulting from the milling.

of a capillary. Furthermore, we accidentally cut into the body of the tip due to the ion beam drifting. Our results are shown in figure 3.10.

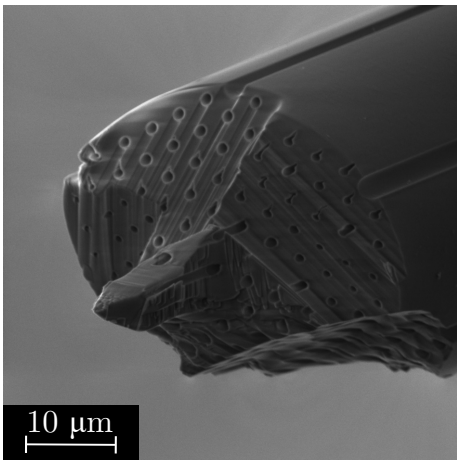

(a) Perspective view.

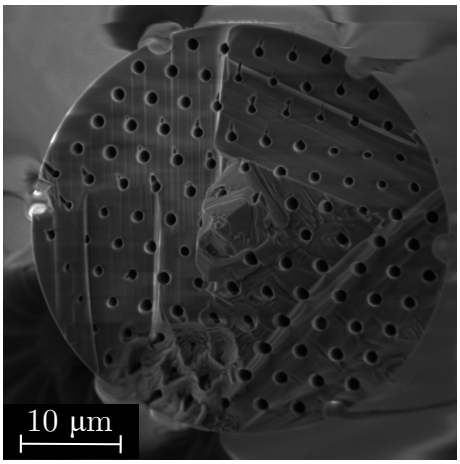

(b) Top view.

Fig. 3.10: SEMs of the first fabricated obelisk tip using the original fibre holder. Tescan LYRA3.

After the first partially successful fabrication of the tip, we acquired the new holder. With the fibre fixed upright relative to the stage in the new holder, we were able to create the central ridge (step (a) in the process depicted on 3.9). The acquired ridge with four out of the six innermost capillaries preserved and with smoothly milled surroundings is shown in figure 3.11. In figure 3.11b it is possible to distinguish between the brighter areas along the ridge, which were milled with the precise milling setup and the darker areas milled with the rough milling preset. Milling with the precise configuration resulted in closing up the capillary outlets.

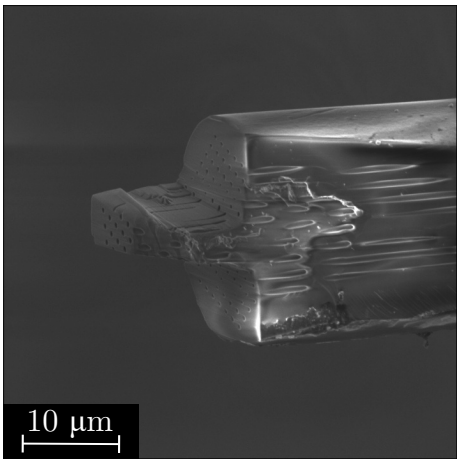

(a) Perspective view.

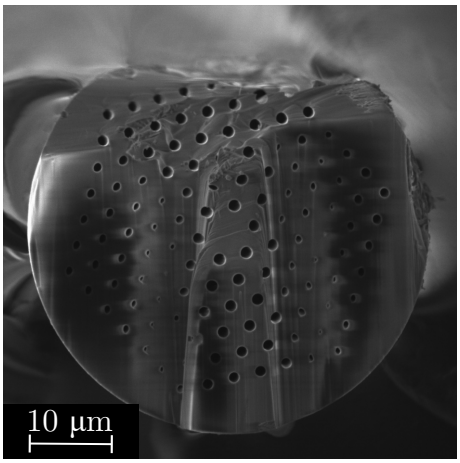

(b) Top view.

Fig. 3.11: SEMs of the ridge resulting from performing the FIB milling according to step (a) in figure 3.9. Tescan LYRA3.

Continuing with the next steps of the described fabrication process, we rotated the fibre and milled out sides of the ridge. Due to a bad selection of the milling area, we milled off too much from one side, leaving us with no other option than to create the column shifted from the core. The column displacement of about 5 µm from the centre of the fibre is shown in figure 3.12b. We proceeded with fabricating the apex, but a drifting beam damaged the column. The uncontrolled milling resulted in a shorter pillar with an extending part in one corner (figure 3.12). We decided not to continue with the apex creation as the column was already too short.

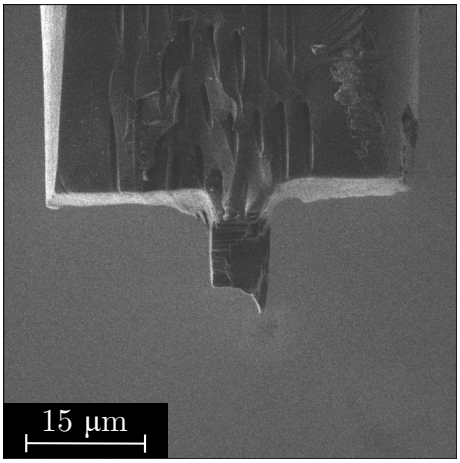

(a) FIB image of side view.

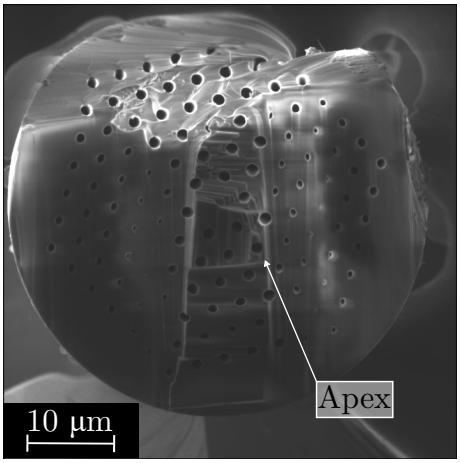

(b) SEM top view.

Fig. 3.12: Second fabricated obelisk tip with a column shifted sideways from the core and poorly crafted apex due to the beam drifting. Tescan LYRA3.

Our proposed fabrication method of the obelisk tip has proven to be excessively time-consuming when performed using the gallium FIB installed within the Tescan LYRA3 electron microscope. In the fabrication process, the biggest difficulty was the drifting of the ion beam leading to milling in the wrong places. This drifting is caused by a charge accumulation in the nonconductive material of the tip. The positively charged surface of the milled material leads to the undesired shift of the ion beam due to the acting repulsive force. We experienced this effect on a greater scale while milling parts of a smaller body — apex creation on the column. This problem could have possibly been overcome by coating the fibre before or during the fabrication process. Although introducing another step into the process would furthermore increase the fabrication time. Considering the tip can be easily destroyed during the fabrication or manipulation with the probe, we do not reckon this process as time effective. The fabrication time might be significantly reduced using a xenon FIB to mill the fibre.

3.1.3 Probe fabrication

Fibres with fabricated tips were with help of Bc. Ondrej Černek glued on a tuning fork in a special manner described in his diploma thesis [55]. In contrast to the depiction of the multifunctional probe concept in figure 3.1 we created probes, for AFM measurement in the shear mode (see figure 3.13). The conventional shear mode was chosen to prove the concept of SEM/SPM correlative measurement with a tip fabricated in a way discussed in section 3.1.2 because probe in this variant is easier to implement into the used electron microscope Tescan VEGA2. As regards the tapping mode probe, the body of the tuning fork in the used electron microscope prevents the electron beam from viewing the sample.

In the case of the first prepared fibre, the stripped part of the fibre was too long, which resulted in Q factor[1] 2650. We will refer to this first fabricated probe with a high Q factor as the O1 probe, which stands for "Obelisk 1" (for the used tip see figure 3.10 and for the concept of the obelisk tip see figure 2.2). The next fabricated probe marked O2 ("Obelisk 2") utilising the second fabricated tip (figure 3.12) has Q factor 310.

Next, in the fabrication process, we would create a golden coating on the probe, but prior to this, the probe would be insulated with a 3 µm layer of parylene using the SCS Labcoter 2 available at CEITEC. Then we could proceed with the deposition of the golden layer using the *Ion Beam Sputtering* (IBS) technique. For this step is in the laboratories of the *Institute of Physical Engineering* (IPE) available a deposition

[1] *Quality factor* (Q factor) describes effective dumping of the resonator. With higher Q factor (lower effective dumping) increases amplitude in the resonance [56].

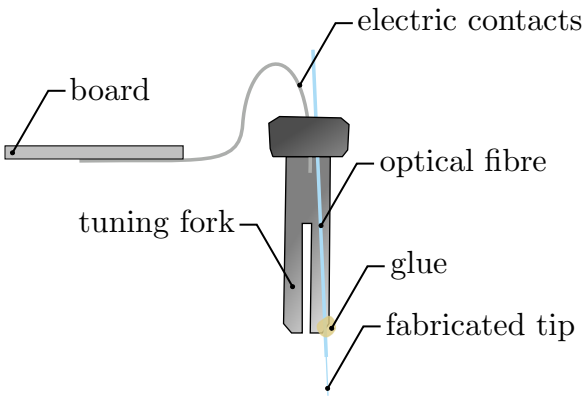

Fig. 3.13: Schematic of the fabricated probe. The optical fibre with the fabricated tip is glued onto the tuning fork. Contacts of the tuning fork are soldered on a board.

apparatus utilising Kaufman ion source [57]. First, a 3 nm thick adhesive layer of Ti would be deposited followed up with a 200 nm thick Au layer. Then the aperture would be fabricated in this coating layer using FIB.

As stated earlier, we focussed only on the SEM/SPM correlative measurements in the practical part and thus we did not proceed with coating the probes with the coating layers.

3.2 Correlative measurements

In this section, we review our measurements with the fabricated probes. With the assistance of our colleague Bc. Ondrej Černek we performed SEM/SPM correlative measurements using Tescan VEGA2 electron microscope with the implemented AFM microscope LiteScope^{TM} available at IPE. The sole purpose of conducting these measurements is to determine whether our fabricated probes are suitable for this application.

The advantage of the SEM/SPM correlative measurements (schematic is depicted in figure 3.14) is in our case the simultaneous acquisition of topography with AFM and surface details with SEM. To obtain both AFM and SEM information from the same area, the probe tip and the electron beam have to be placed close to each other. Ideally, both should remain static with a constant distance from each other and the scanning of the sample is done by moving with the piezoelectric scanner.

As the sample for the testing measurements was chosen a calibration grating TGZ2 with parallel ridges with height 107 ± 2 nm and period 3 µm [58].

The first measurement was carried out with the O1 probe and because of the relatively high Q factor (2650), the frequency modulation regime was chosen. Due

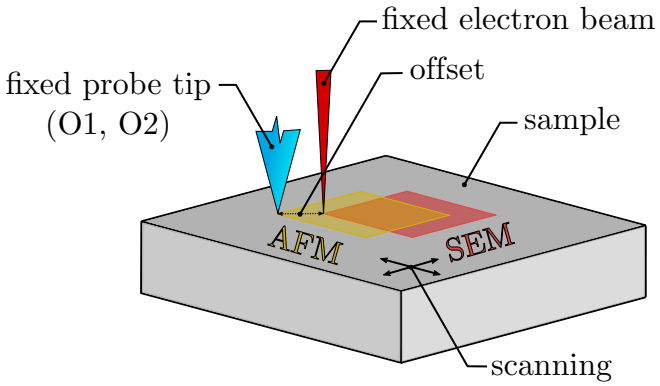

Fig. 3.14: Schematic of the SEM/SPM correlative measurements with marked a offset between the probe tip and the electron beam. The offset dictates the overlap of AFM and SEM scanning windows. The probe tip (O1, O2) and the electron beam are fixed and the scanning is done with the sample.

to the short tip on the fibre, we were not able to view the close surroundings of the tip with SEM (see figure 3.15b). A large offset (12.5 µm) of the electron beam from the tip was set to place the beam on the sample. Shifting the electron beam further from the tip resulted in a smaller overlapping area, where both AFM and SEM images were acquired. In figure 3.15b, the original positions of the tip and electron beam were in the upper left corner of their respective scanning windows.

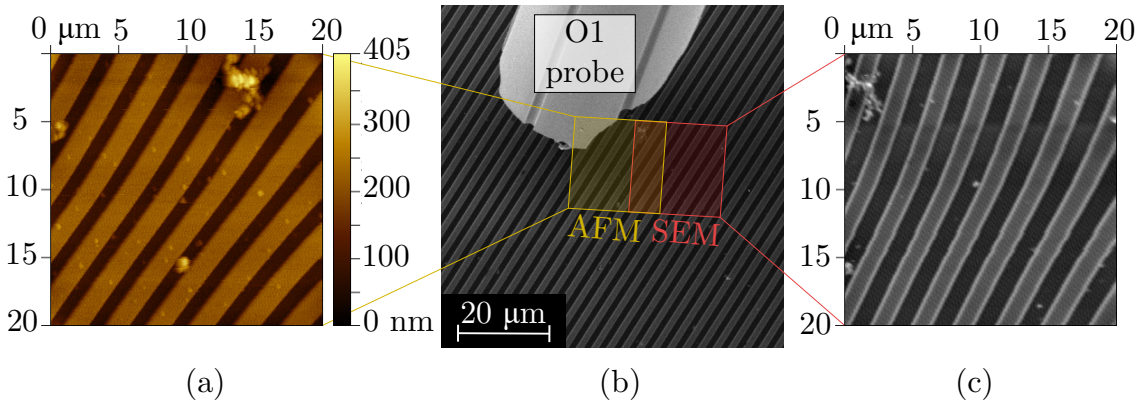

Fig. 3.15: SEM/SPM correlative measurement with O1 probe (see figure 3.10 for the tip image and section 3.1.3 for detailed information) of TGZ2 calibration grating. (a) AFM topography acquired during the correlative measurements. (b) SEM of the fibre end with hidden tip and marked off AFM and SEM scanning areas on the grating. (c) SEM acquired during the correlative measurements. LiteScope^{TM} and Tescan VEGA2.

Simultaneously acquired AFM and SEM images are shown in figures 3.15 (a)

and (c), respectively. AFM image is distorted by the hysteresis of the piezoelectric scanner, resulting in the uneven spacing of the lines in the right part of the image. The right edges of the ridges are sharper because they were the leading edges in the depicted topography[2]. By reviewing the topography profile in the upper left region and averaging over 20 pixels, we measured the step height as 133 nm and the period as 2.7 µm. Some impurity was probably present on the top of the tip, acting like a sharper tip as a result. In the SEM image, there are visible bright edges of the ridges. Higher contrast at the edges is caused by the so-called edge effect — higher SE yield at the edges compared to plane surfaces [59]. Curved edges are caused by the drifting electron beam, which did not stay at a constant distance from the tip during the measurement.

For better visualisation, it is possible to represent the acquired topography in a 3D view[3] as shown in figure 3.16.

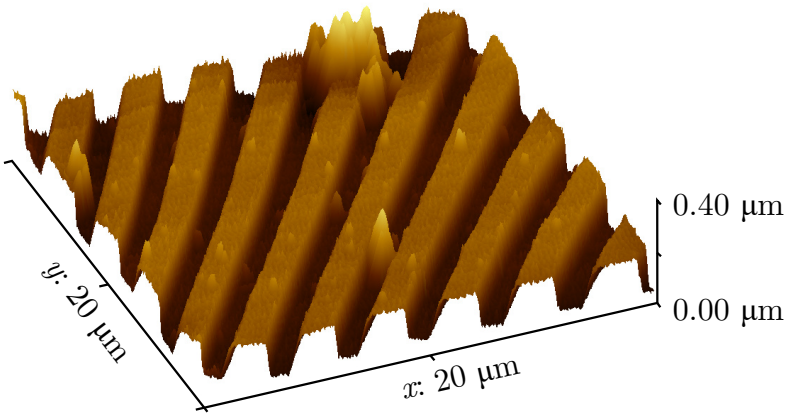

Fig. 3.16: 3D visualisation of the measured topography with the O1 probe. LiteScope™.

The second measurement was done with the O2 probe in an amplitude modulation regime. We were not able to point the electron beam on the sample close to the tip, likewise in the case of the previous probe. The acquired AFM image (figure 3.17a) is distorted with heavy noise, this might be due to the tip being bifurcated. Once again, widening of the ridges is present in both images (figure 3.17 (a) and (c)) caused by the hysteresis of the piezoelectric motors. By measuring the topography in the upper left corner and averaging over 20 pixels, we acquired the height of the step 136 nm and period 2.4 µm.

[2]During the performed top-down scanning all lines are scanned twice. First, from the left to the right and then vice versa — resulting in two topographies differing in the scanning direction.

[3]Additionally for applicable samples the (3D) topography could be overlaid with SEM.

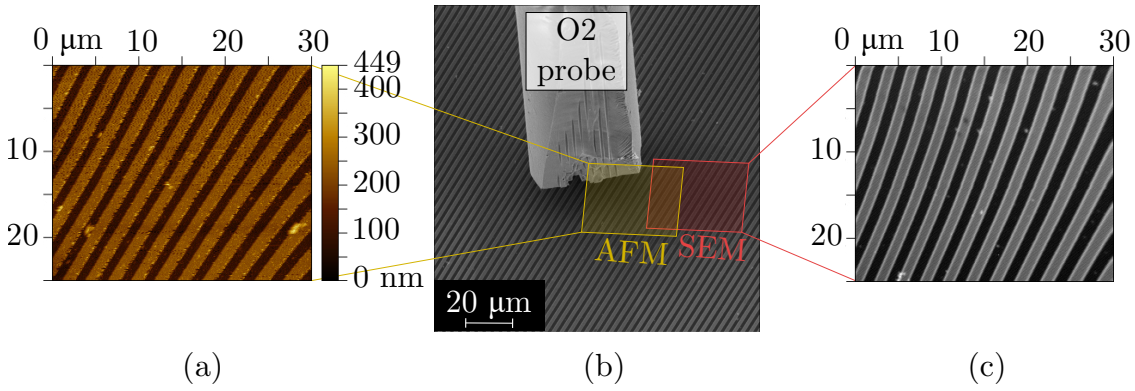

Fig. 3.17: SEM/SPM correlative measurement with O2 probe (see figure 3.12 for the tip image and section 3.1.3 for detailed information) of TGZ2 calibration grating. (a) AFM topography acquired during the correlative measurement. (b) SEM of the fibre end with hidden tip and marked off AFM and SEM scanning areas on the grating. (c) SEM acquired during the correlative measurement. LiteScope^{TM} and Tescan VEGA2.

With both probes, we were able to perform correlative SEM/SPM measurements, but the acquired images overlap only partially. Better results might be achieved by altering the tip design and making it possible to place the tip and electron beam close to each other on the sample. Nevertheless, we deem our results as a proof-of-concept. Dimensions of the grating in both cases match the dimensions listed by the manufacturer in the order of magnitude. The step height and the period of the grating are with both probes measured smaller than they are said to be by the manufacturer. Tips on both probes are probably not sharp enough to follow the true topography profile.

We managed to create a draft of the multifunctional probe for the correlative SEM/SPM measurements, develop fabrication methodology and perform the desired measurements with the fabricated probe. With the proof-of-concept successfully acquired we now plan to move on to the tapping variant of the probe and further improve and make faster the fabrication process. Furthermore, the more advanced functionalities will be introduced within the TACR project FW03010504 — Development of in-situ techniques for characterization of materials and nanostructures.

Conclusion

In this work, we presented our draft of the possible multifunctional probe for the correlative SEM/SPM measurements. The key element of the fabricated probe as well as this work is the HC-PCF optical fibre. The cladding of this fibre includes a microstructured region with capillaries. We focussed on the possibility of utilising these hollow channels to provide more functionality. Within the research study, we covered topics concerning the tip fabrication on a fibre of a like nature, the introduction of working fluids through the capillaries, and manufacture of the capillary wires. Information acquired in the research was taken into account and partially is a subject of our future plans.

We decided to fabricate the tip on the fibre using the combined forces of the wet etching with HF and the FIB milling. Based on the FDTD simulations of a light guidance capability was one of the three presented designs chosen for the fabrication. To etch the fibre and avoid the destruction of the internal structure, we developed the drop etching technique. The fabrication process using FIB milling was introduced and put into practice. The whole concept was then verified with conducted correlative measurements. Nevertheless, a few flaws we have encountered leave space for improvement. The time inefficiency of the fabrication process could be significantly improved using a Xe FIB instead of the Ga one we used. The reduced time demandingness would make it possible to effectively add one more step into the fabrication process — coating with a golden layer before or during the fabrication. Milling the fibres covered with a surface conductive layer would resolve the beam drifting issues caused by the charge accumulation in the nonconductive sample. Lastly, an alternation of the tip design in a way allowing close placement of the electron beam is desirable. This would be beneficial for the correlative measurements, as it would lead to more overlapping areas in the SPM and SEM images.

We plan on continuing with further work on the concept of a multifunctional probe for the correlative measurements. Successful fabrication of such probe would make it possible to perform different measurements and alter or even fabricate nanostructures in-situ of the electron microscope. The decision, whether this work contributes to the efforts of extending the boundaries mentioned in the introduction or does not even come close to them, is left upon the reader. However, we do believe that the work that has never been started is the last to finish and that the road goes on and on [60].

Bibliography

[1] ZWORYKIN, V. K. The scanning electron microscope. *Scientific American*. **1942**, 167(3), pp. 111-113.

[2] BINNIG, G. and ROHRER, H. Scanning tunneling microscopy. *Surface Science*. **1982**. 126(1-3). pp. 236-244.

[3] BINNIG, G. and QUATE, C. F. Atomic force microscope. *Physical Review Letters*. **1986**. 56(9), pp. 930-934.

[4] NEUMAN, J. *et al.* Correlative probe and electron microscopy CPEM^{TM} – The novel technology for 3D material surface analysis. *Microscopy and Microanalysis*. **2019**. 25(2), pp. 430–431. doi:10.1017/S1431927619002885.

[5] BOBEK, J. *Příprava a testování SNOM sond speciálních vlastností*. Brno, **2019**. Master's Thesis. 62 p. Brno University of Technology, Faculty of Mechanical Engineering. Supervised by prof. RNDr. Jiří Spousta, PhD.

[6] ČERNEK, O. *Využití speciálního optického vlákna v komoře elektronového mikroskopu*. Brno, **2019**. Bachalor's Thesis. 43 p. Brno University of Technology, Faculty of Mechanical Engineering. Supervised by Ing. Michal Pavera, PhD.

[7] HUSZKA, G. and GIJS, M. A. M. Super-resolution optical imaging: A comparison. *Micro and Nano Engineering*. **2019**. 2, pp. 7–28. doi:10.1016/j.mne.2018.11.005.

[8] WEISENBURGER, S. and SANDOGHDAR, V. Light microscopy: An ongoing contemporary revolution. *Contemporary Physics*. **2015**. 56(2), pp. 123–143. doi:10.1080/00107514.2015.1026557.

[9] BAZYLEWSKI, P., EZUGWU, S. and FANCHINI, G. A Review of three-dimensional scanning near-field optical microscopy (3D-SNOM) and its applications in nanoscale light management. *Applied Sciences*. **2017**. 7(10), pp. 973-996. doi:10.3390/app7100973.

[10] ROTENBERG, N. and KUIPERS, L. Mapping nanoscale light fields. *Nature Photonics*. 2014. 8(12), pp. 919–926. doi:10.1038/nphoton.2014.285.

[11] POLI, F., CUCINOTTA, A. and SELLERI, S. *Photonic crystal fibers: Properties and applications*. Dordrecht: Springer, **2007**. p. 11. Springer series in materials science, 102. ISBN: 978-1-4020-6326-8.

[12] CARLSON, C. A. and WOEHL, J. C. Fabrication of optical tips from photonic crystal fibers. *Review of Scientific Instruments*. **2008**. 79(10), p. 103707. doi:10.1063/1.3002427.

[13] RUSSELL, P. Photonic crystal fibers. *Science*. **2003**. 299(5605), pp. 358–362. doi:10.1126/science.1079280.

[14] AT&T Bell Laboratories Inc. Etch procedure for optical fibers. United States. C03C15/00. US4469554A. 05.04.**1983**.

[15] STÖCKLE, R. *et al.* High-quality near-field optical probes by tube etching. *Applied Physics Letters*. **1999**. 75(2), pp. 160–162. doi:10.1063/1.124305.

[16] HABER, L. H. *et al.* Shape control of near-field probes using dynamic meniscus etching. *Journal of Microscopy*. **2004**. 214(1), pp. 27–35. doi:10.1111/j.0022-2720.2004.01308.x.

[17] SHI, J. and QIN, X. R. Formation of glass fiber tips for scanning near-field optical microscopy by sealed- and open-tube etching. *Review of Scientific Instruments*. **2005**. 76(1), p. 013702. doi:10.1063/1.1823778.

[18] PURA, P. *et al.* Polymer microtips fabricated at the extremity of photonic crystal fibers. *Journal of Materials Science and Engineering: B*. **2013**. 3(12), pp. 749-758. doi:10.17265/2161-6221/2013.12.001.

[19] DVOŘÁK, P. *Nanofotonika*. Brno, **2018**. PhD Thesis. 134 p. Brno University of Technology, Faculty of Mechanical Engineering. Supervised by prof. RNDr. Tomáš Šikola, CSc.

[20] KLEINDIEK NANOTECHNIK. *SEM-compatible glue* [online]. [Accessed 2021-4-20]. Available at: https://www.nanotechnik.com/semglu.html.

[21] TESCAN. *Tescan Nanomanipulator* [online]. [Accessed 2021-5-12]. Available at: https://www.tescan.com/product/tescan-nanomanipulator/.

[22] DORVAL DION, C.A. and TAVARES, J.R. Photo-initiated chemical vapor deposition as a scalable particle functionalization technology (a practical review). *Powder Technology*. **2013**. 239, pp 484–491. doi:10.1016/j.powtec.2013.02.024.

[23] HUTH, M. *et al.* Focused electron beam induced deposition: A perspective. *Beilstein Journal of Nanotechnology*. **2012**. 3, pp. 597–619. doi:10.3762/bjnano.3.70.

[24] DONGARI, N., SHARMA, A. and DURST, F. Pressure-driven diffusive gas flows in micro-channels: from the Knudsen to the continuum regimes. *Microfluidics and Nanofluidics*. **2009**. 6(5), pp. 679–692. doi:10.1007/s10404-008-0344-y.

[25] CHAMBERS, A. *Modern vacuum physics*. Boca Raton: Chapman & Hall/CRC, **2005**. p. 26. Masters series in physics and astronomy, 4. ISBN: 978-0-8493-2438-3.

[26] KARNIADAKIS, G., BESKOK, A. and ALURU, N. *Microflows and nanoflows*. New York: Springer-Verlag, **2005**. p. 16, 57. Interdisciplinary Applied Mathematics, 28. ISBN: 978-0-387-22197-7.

[27] AISSA, A. *et al.* Pressure-driven gas flows in micro channels with a slipBoundary: A numerical investigation.*Fluid Dynamics & Materials Processing*. **2020**. 16(2), pp. 147–159. doi:10.32604/fdmp.2020.04073.

[28] OSTADFAR, A. Fluid mechanics and biofluids principles. In: *Biofluid Mechanics*. London: Academic Press, **2016**. p. 22. ISBN: 978-0-12-802408-9.

[29] AKTAS, O., ALURU, N. R. and RAVAIOLI, U. Application of a parallel DSMC technique to predict flow characteristics in microfluidic filters. *Journal of Microelectromechanical Systems*. **2001**. 10(4), pp. 538–549. doi:10.1109/84.967377.

[30] DONGARI, N. and AGRAWAL, A. Modeling of Navier–Stokes equations for high Knudsen number gas flows. *International Journal of Heat and Mass Transfer*. **2012**. 55(15–16), pp. 4352–4358. doi:0.1016/j.ijheatmasstransfer.2012.04.002.

[31] BESKOK, A. and KARNIADAKIS, E. M. Report: A model for flows in channels, pipes, and ducts at micro and nano scales. *Microscale Thermophysical Engineering*. **1999**. 3(1), pp. 43–77. doi:10.1080/108939599199864.

[32] SHEN, C., MAYINGER, F. and MEWES, D. *Rarefield gas dynamics fundamentals*, Simulations and Micro Flows. Berlin: Springer-Verlag Berlin Heidelberg, **2005**. p. 159. ISBN: 978-3-540-27230-4.

[33] ZHAO, Y. *et al.* Review on structures and principles of gas cells in the absorption spectrum–based optical fiber gas sensor systems. *Instrumentation Science & Technology*. **2012**. 40(5), pp. 385–401. doi:10.1080/10739149.2012.679720.

[34] BENABID, F. *et al.* Compact, stable and efficient all-fibre gas cells using hollow-core photonic crystal fibres. *Nature*. **2005**. 434(7032), pp. 488–491. doi:10.1038/nature03349.

[35] DICAIRE, I., BEUGNOT, J.-C. and THÉVENAZ, L. Analytical modeling of the gas-filling dynamics in photonic crystal fibers. *Applied Optics*. **2010**. 49(24), p. 4604. doi:10.1364/AO.49.004604.

[36] HENNINGSEN, J. and HALD, J. Dynamics of gas flow in hollow core photonic bandgap fibers. *Applied Optics*. **2008**. 47(15), p. 2790. doi:10.1364/AO.47.002790.

[37] HOO, Y. L. *et al.* Measurement of gas diffusion coefficient using photonic crystal fiber. *IEEE Photonics Technology Letters*. **2003**. 15(10), pp. 1434–1436. doi:10.1109/LPT.2003.818241.

[38] PARMAR, V. and BHATNAGAR, R. Analysis of gas flow dynamics in hollow core photonic crystal fibre based gas cell. *Optik*. **2014**. 125(13), pp. 3204–3208. doi:0.1016/j.ijleo.2014.01.022.

[39] NKT Photonics. *HC-1550-02* [online]. [Accessed 2021-4-6]. Available at: https://www.nktphotonics.com/wp-content/uploads/sites/3/2015/01/hc-1550-02.pdf?1552227160.

[40] HENSLEY, C. *et al.* Photonic band-gap fiber gas cell fabricated using femtosecond micromachining. *Optics Express*. **2007**. 15(11), p. 6690. doi:10.1364/OE.15.006690.

[41] VAN BRAKEL, A. *et al.* Micro-channels machined in microstructured optical fibers by femtosecond laser. *Optics Express*. **2007**. 15(14), p. 8731. doi:10.1364/OE.15.008731.

[42] CYTOSURGE. *FluidFM^{TM} probes* [online]. [Accessed 2021-5-3]. Available at: https://www.cytosurge.com/probes#.

[43] VENTRICI DE SOUZA, J. *et al.* Three-dimensional nanoprinting via direct delivery. *The Journal of Physical Chemistry B*. **2018**. 122(2), pp. 956–962. doi:10.1021/acs.jpcb.7b06978.

[44] LEE, H. W. *et al.* Pressure-assisted melt-filling and optical characterization of Au nano-wires in microstructured fibers. *Optics Express*. **2011**. 19(13), p. 12180. doi:10.1364/OE.19.012180.

[45] MOHAMMED, M. G. and KRAMER, R. All-printed Flexible and Stretchable Electronics. *Advanced Materials*. **2017**. 29(19), p. 1604965. doi:10.1002/adma.201604965.

[46] YOON, J. *et al.* Design and fabrication of novel stretchable device arrays on a deformable polymer substrate with embedded liquid-metal interconnections. *Advanced Materials*. **2014**. 26(38), pp. 6580–6586. doi:10.1002/adma.201402588.

[47] STROUSE, G.F. *Standard Reference Material 1751: Gallium Melting-Point Standard*. Washington: U. S. Government Printing Office, **2004**. p. 18. 260, 157.

[48] LIN, Y., GORDON, O. and KHAN, M. R. Vacuum filling of complex microchannels with liquid metal. *Lab On a Chip*. **2017**, 17(18), pp. 3043-3050. doi:10.1039/C7LC00426E.

[49] NKT Photonics. *Large mode area photonic crystal fibers* [online]. [Accessed 2021-2-29]. Available at: https://www.nktphotonics.com/lasers-fibers/product/large-mode-area-photonic-crystal-fibers/.

[50] NIELSEN, M. D. *et al.* Bandwidth comparison of photonic crystal fibers and conventional single-mode fibers. *Optics Express*. **2004**. 12(3), pp. 430-435. doi:0.1364/OPEX.12.000430.

[51] NOVOTNA, V. *et al.* AFM-in-SEM as a tool for comprehensive sample surface analysis. *Microscopy Today*. **2020**. 28(3), pp. 38–46. doi:10.1017/S1551929520000875.

[52] THORLABS. *Three-hole stripping tool for fiber buffers and jackets* [online]. [Accessed 2021-3-20]. Available at: https://www.thorlabs.com/thorproduct.cfm?partnumber=FTS4.

[53] THORLABS. *Ruby dualscribe fiber optic scribe* [online]. [Accessed 2021-3-20]. Available at: https://www.thorlabs.com/thorproduct.cfm?partnumber=S90R.

[54] KRPENSKÝ, J. *Interakce mezi SNOM hrotem a blízkým elektromagnetickým polem*. Brno, **2020**. Bachalor's Thesis. 53 p. Brno University of Technology, Faculty of Mechanical Engineering. Supervised by Ing. Petr Dvořák, PhD.

[55] ČERNEK, O. *Korelativní měření katodoluminiscence za použití technik SEM a SPM*. Brno, **2021**. Master's Thesis. 60 p. Brno University of Technology, Faculty of Mechanical Engineering. Supervised by prof. RNDr. Jiří Spousta, PhD.

[56] CHEN, L., YU, X. and WANG, D. Cantilever dynamics and quality factor control in AC mode AFM height measurements. *Ultramicroscopy*. **2007**. 107(4–5), pp. 275–280. doi:10.1016/j.ultramic.2006.06.006.

[57] KAUFMAN, H. R. and ROBINSON, R. S. Ion source design for industrial applications. *AIAA Journal*. **1982**. 20(6), pp. 745–760. doi:10.2514/3.51131.

[58] NT-MDT SPECTRUM INSTRUMENTS. *TGZ2* [online]. [Accessed 2021-5-6]. Available at: http://ntmdt-tips.com/products/view/tgz2.

[59] SEILER, H. Secondary electron emission in the scanning electron microscope. *Journal of Applied Physics*. **1983**. 54(11), p. R1–R18. doi:10.1063/1.332840.

[60] TOLKIEN, J. R. R. *The Fellowship of the Ring*. London: HarperCollins, **2005**. p. 62, 438 ISBN: 978-0-00-720354-3.

List of symbols, quantities and abbreviations

AFM Atomic Force Microscopy

BSE Backscattered Electrons

CEITEC Central European Institute of Technology

CPEM Correlative Probe and Electron Microscopy

DSMC Direct Simulation Monte Carlo

FDTD Finite-Difference Time-Domain

FEBID Focused Electron Beam Induced Deposition

FIB Focused Ion Beam

FIBID Focused Ion Beam Induced Deposition

GIS Gas Injection System

HC-PCF Hollow-Core Photonic Crystal Fibre

HF hydrofluoric acid

IBS Ion Beam Sputtering

IPE Institute of Physical Engineering

IR Infrared

MSIF Modified Step Index Fiber

PDMS poly(dimethylsiloxane)

PE Primary Electrons

Q factor Quality factor

SC-PCF Solid-Core Photonic Crystal Fibre

SE Secondary Electrons

SEM Scanning Electron Microscope

SNOM Scanning Near-field Optical Microscopy

SPM Scanning Probe Microscopy

STM Scanning Tunneling Microscope